



Discovery of *N*-[5-({2-[(cyclopropylcarbonyl)amino]imidazo[1,2-*b*]pyridazin-6-yl}oxy)-2-methylphenyl]-1,3-dimethyl-1*H*-pyrazole-5-carboxamide (TAK-593), a highly potent VEGFR2 kinase inhibitor

Naoki Miyamoto, Nozomu Sakai, Takaharu Hirayama, Kazuhiro Miwa, Yuya Oguro, Hideyuki Oki, Kengo Okada, Terufumi Takagi, Hidehisa Iwata, Yoshiko Awazu, Seiji Yamasaki, Toshiyuki Takeuchi, Hiroshi Miki, Akira Hori, Shinichi Imamura*

Pharmaceutical Research Division, Takeda Pharmaceutical Company Limited, 2-26-1 Muraokahigashi, Fujisawa, Kanagawa 251-8555, Japan

ARTICLE INFO

Article history:

Received 27 December 2012

Revised 30 January 2013

Accepted 31 January 2013

Available online 13 February 2013

Keywords:

VEGF

VEGFR2

Kinase inhibitor

Imidazo[1,2-*b*]pyridazine

ABSTRACT

Vascular endothelial growth factor (VEGF) plays important roles in tumor angiogenesis, and the inhibition of its signaling pathway is considered an effective therapeutic option for the treatment of cancer. In this study, we describe the design, synthesis, and biological evaluation of 2-acylamino-6-phenoxy-imidazo[1,2-*b*]pyridazine derivatives. Hybridization of two distinct imidazo[1,2-*b*]pyridazines **1** and **2**, followed by optimization led to the discovery of *N*-[5-({2-[(cyclopropylcarbonyl)amino]imidazo[1,2-*b*]pyridazin-6-yl}oxy)-2-methylphenyl]-1,3-dimethyl-1*H*-pyrazole-5-carboxamide (**23a**, TAK-593) as a highly potent VEGF receptor 2 kinase inhibitor with an IC_{50} value of 0.95 nM. The compound **23a** strongly suppressed proliferation of VEGF-stimulated human umbilical vein endothelial cells with an IC_{50} of 0.30 nM. Kinase selectivity profiling revealed that **23a** inhibited platelet-derived growth factor receptor kinases as well as VEGF receptor kinases. Oral administration of **23a** at 1 mg/kg bid potently inhibited tumor growth in a mouse xenograft model using human lung adenocarcinoma A549 cells ($T/C = 8\%$).

© 2013 Elsevier Ltd. All rights reserved.

1. Introduction

Angiogenesis is the formation of new capillary blood vessels from existing vasculature. Tumor growth is dependent on the nutrients and oxygen delivered by the vessels formed during angiogenesis.¹ Vascular endothelial growth factor (VEGF) signaling through VEGF receptor 2 (VEGFR2, also known as KDR) has been shown to play a major role in the regulation of tumor angiogenesis.^{2,3} Expression of VEGF is enhanced in several types of human tumors, and its expression levels correlate with poor prognosis and clinical stage in patients with solid tumors.^{4–11} Therefore, VEGF/VEGFR2 signaling is an attractive therapeutic target in the treatment of cancer. A humanized anti-VEGF monoclonal antibody (bevacizumab)¹² and several small molecule VEGFR2 kinase inhibitors (sorafenib,¹³ sunitinib,¹⁴ pazopanib,¹⁵ and axitinib¹⁶) have been approved as antiangiogenic drugs, and they have shown clinical benefits in the treatment of some tumors, with manageable side effects. Many other new angiogenesis inhibitors are being evaluated in clinical trials.¹⁷ Following the formation of new tumor vessels, pericyte recruitment is an essential step leading to

increased stability of immature tumor vessels. Platelet-derived growth factor (PDGF)-B/PDGF receptor β (PDGFR β) signaling is necessary for pericyte recruitment during angiogenesis.¹⁸ It has also been suggested that inhibition of PDGF/PDGFR signaling is an effective way to block further growth of end-stage tumors.¹⁹ In addition to stabilizing tumor vessels, expression of PDGF has been known to correlate with autocrine stimulation of both tumor growth and the recruitment of tumor stroma fibroblasts.²⁰ Consequently, it is conceivable that simultaneous inhibition of VEGFR2 and PDGFR kinases may lead to synergistic antiangiogenic effects in tumor therapy.

We previously reported that the 6-phenoxy-imidazo[1,2-*b*]pyridazine derivative **1**, possessing a benzamide unit, functions as a VEGFR2 kinase inhibitor (Fig. 1).²¹ Compound **1** showed potent VEGFR2 kinase inhibitory activity with an IC_{50} value of 7.1 nM. However, it only modestly suppressed VEGF-stimulated proliferation of human umbilical vein endothelial cells (HUVEC) with an IC_{50} of 650 nM. Meanwhile, searching our compound library of inhibitors targeting other kinases, we found that the 2-acylamino-imidazo[1,2-*b*]pyridazine derivative **2** moderately inhibited VEGFR2 kinase ($IC_{50} = 1300$ nM). To determine its mode of binding to VEGFR2 kinase, the X-ray crystal structure of VEGFR2 complexed with **2** was solved using a soaking method (Fig. 2a). The N1-nitrogen of the imi-

* Corresponding author. Tel.: +81 466 32 1166; fax: +81 466 29 4448.

E-mail address: shin-ichi.imamura@takeda.com (S. Imamura).

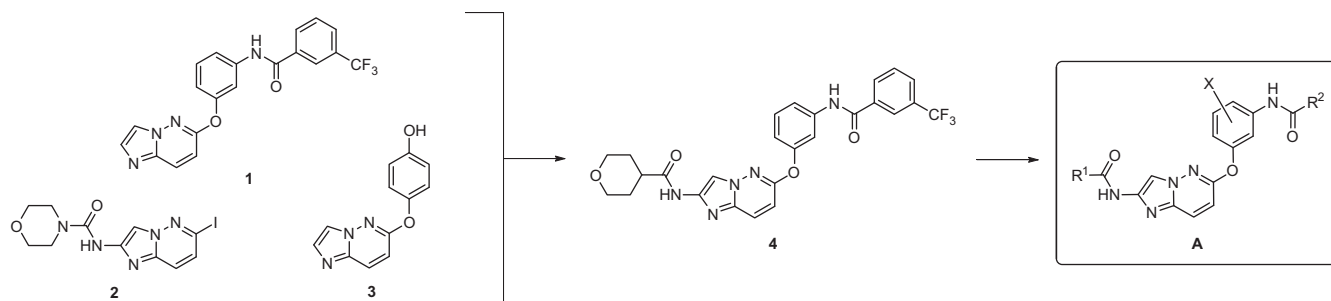
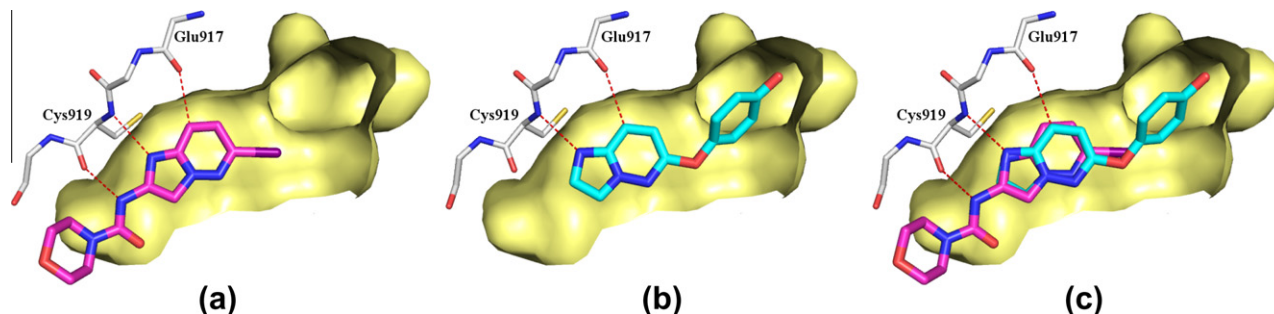


Figure 1. Design of hybrid compound A.

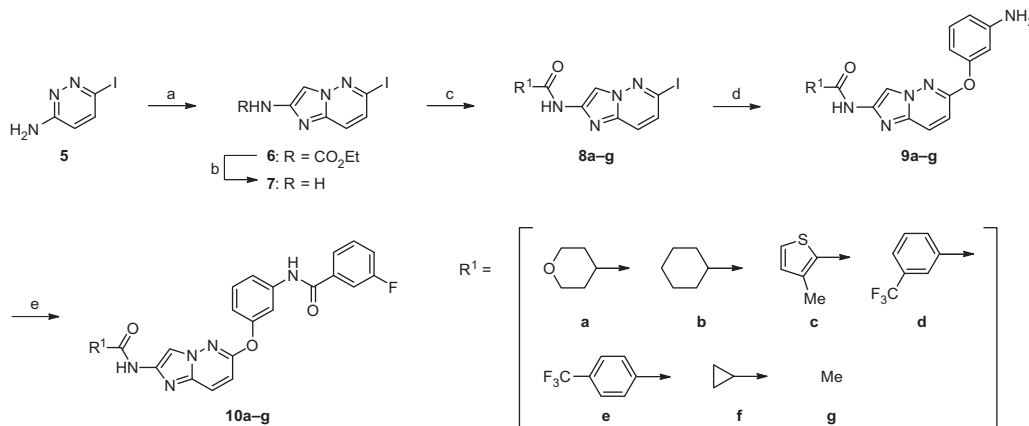
Figure 2. (a) Binding mode of **2** to VEGFR2. (b) Binding mode of **3** to VEGFR2. (c) Superposition of **2** (pink) and **3** (blue). Dashed lines represent hydrogen bonds.

dazo[1,2-*b*]pyridazine forms a hydrogen bonding interaction with the NH group of Cys919 in the VEGFR2 hinge region, and the iodine atom at the 6-position is located near the entrance of the back pocket. The CH proton at the 8-position interacts with the carbonyl group of Glu917. The acylamino group at the 2-position is situated in the solvent accessible region, where the NH group interacts with the carbonyl group of Cys919. In addition, the 6-phenoxy-imidazo[1,2-*b*]pyridazine **3** was identified by fragment library screening as a weak binding fragment of VEGFR2 kinase.²² Its binding mode was determined by X-ray crystallography (Fig. 2b), and the binding modes of the imidazo[1,2-*b*]pyridazine cores in **2** and **3** were found to be virtually identical (Fig. 2c). Based on the structural resemblance of **1** to **3**, it was speculated that the imidazo[1,2-*b*]pyridazine group of **1** would be located at the same site. In that case, the benzamide moiety of **1** would occupy the back pocket, and the solvent accessible region would remain vacant. We hypothesized that the introduction of an NH group at the 2-position of the imidazo[1,2-*b*]pyridazine in **1** would provide an additional hydrogen bonding site with the carbonyl oxygen of Cys919, which might en-

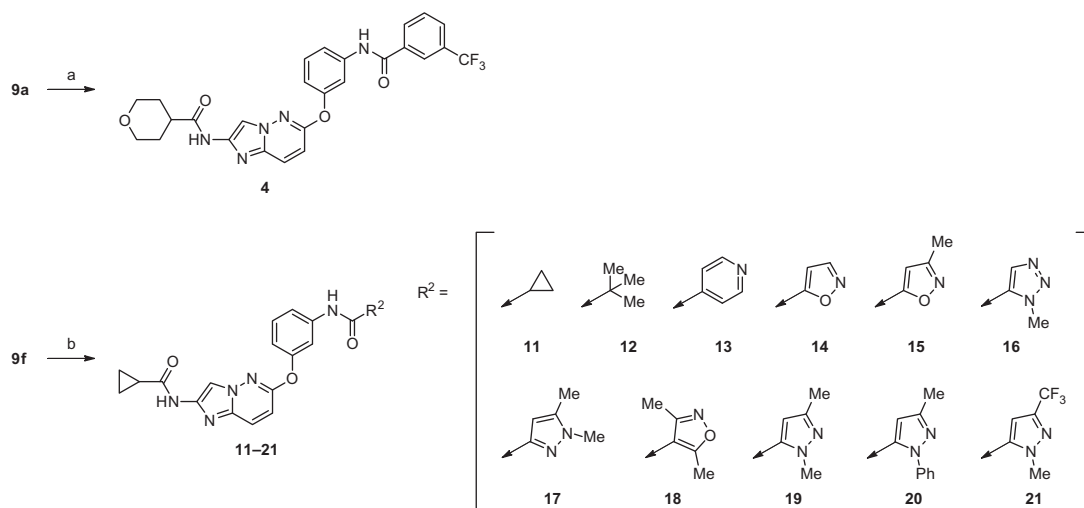
hance the interaction between the inhibitor and VEGFR2. As we predicted, the hybrid compound **4** potentially inhibited VEGFR2 kinase activity (IC_{50} = 6.9 nM). Furthermore, **4** was found to strongly suppress the growth of HUVEC (IC_{50} = 9.1 nM). Encouraged by these results, we designed compounds of type **A** in order to discover VEGFR2 kinase inhibitors with potent cellular activity, as well as physicochemical properties suitable for oral administration. In this study, we report the synthesis, structure–activity relationships (SAR), and characterization of these new inhibitors.

2. Chemistry

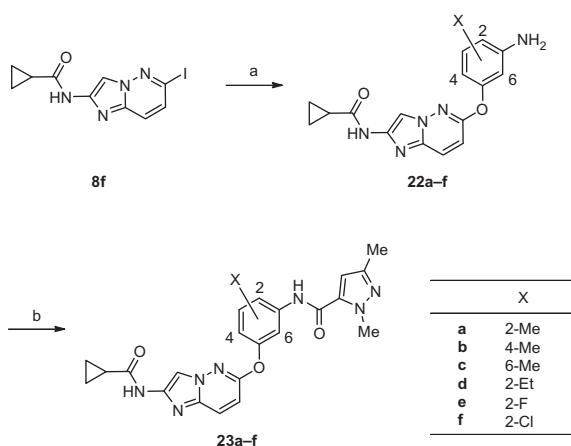
Target compounds were prepared according to the synthetic routes shown in Schemes 1–3. Scheme 1 shows the synthesis of the 2-acylamino-6-phenoxyimidazo[1,2-*b*]pyridazine derivatives **10a–g**. Ring formation of 3-amino-6-iodopyridazine (**5**) with ethyl (chloroacetyl)carbamate in the presence of Na_2HPO_4 afforded the 6-iodoimidazo[1,2-*b*]pyridazine **6**. Removal of the ethoxycarbonyl group of **6** using aqueous $Ba(OH)_2$ gave the amine **7**, which was re-



Scheme 1. Reagents: (a) ethyl (chloroacetyl)carbamate, Na_2HPO_4 , DMA; (b) $Ba(OH)_2$, NMP/ H_2O ; (c) R^1COCl , DMA; (d) 3-aminophenol, K_2CO_3 , DMF; (e) 3-fluorobenzoyl chloride, DMA.



Scheme 2. Reagents: (a) 3-(trifluoromethyl)benzoyl chloride, DMA; (b) $R^2\text{COCl}$, DMA.



Scheme 3. Reagents: (a) aminophenols, K_2CO_3 , DMF for **22a,c-f**; 5-amino-2-methylphenol, NaH, DMF for **22b**; (b) 1,3-dimethyl-1H-pyrazole-5-carbonyl chloride, DMA for **23a,e,f**; 1,3-dimethyl-1H-pyrazole-5-carbonyl chloride, Et_3N , THF for **23b,c**; 1,3-dimethyl-1H-pyrazole-5-carbonyl chloride, NMP for **23d**.

acted with a variety of acid chlorides in *N,N*-dimethylacetamide (DMA) to provide the corresponding amides **8a–g**. Substitution of the iodine atom in **8a–g** by 3-aminophenol produced the anilines **9a–g**, which were acylated with 3-fluorobenzoyl chloride to give the amides **10a–g**.

The aniline **9a** was also converted into the 3-(trifluoromethyl)benzamide derivative **4** by treatment with 3-(trifluoromethyl)benzoyl chloride in DMA (Scheme 2). In addition, compounds possessing various acyl groups (**11–21**) were synthesized by reaction of **9f** with the corresponding acid chlorides.

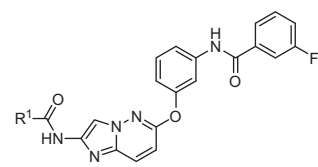
Compounds having a substituent (X) on the central phenyl ring (**23a–f**) were synthesized as shown in Scheme 3. The 6-iodoimidazo[1,2-*b*]pyridazine **8f** was coupled with appropriate aminophenols to give the corresponding anilines **22a–f**. Treatment of **22a–f** with 1,3-dimethyl-1H-pyrazole-5-carbonyl chloride afforded the corresponding amides **23a–f**.

3. Results and discussion

The imidazo[1,2-*b*]pyridazine derivatives depicted in Tables 1–3 were evaluated for their inhibitory activity against VEGFR2 by a non-RI assay using the AlphaScreen system.²³ Subsequently, a cell

Table 1

Effect of the amide substituent R^1 on VEGFR2 kinase inhibitory activity^a



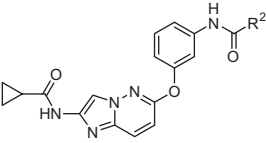
Compound	R^1	VEGFR2 IC_{50} (nM)
4^b		6.9 (6.4–7.4)
10a		2.7 (2.6–2.9)
10b		11 (10–12)
10c		19 (16–21)
10d		160 (120–200)
10e		120 (110–140)
10f		1.0 (0.96–1.1)
10g	Me	1.1 (1.0–1.2)

^a Numbers in parentheses represent 95% confidence interval.

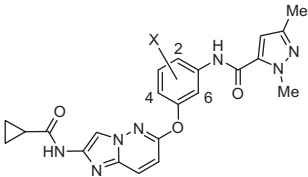
^b See Figure 1 for the structure of **4**.

proliferation assay was performed to determine the ability of VEGFR2 inhibitors to suppress VEGF-stimulated growth of HUVEC.

A preliminary study revealed that the 3-fluorobenzamide derivative **10a** (IC_{50} = 2.7 nM) showed more potent VEGFR2 kinase inhibitory activity than that of **4** (IC_{50} = 6.9 nM). Thus, optimization of the amide substituent R^1 at the 2-position of the imidazo[1,2-*b*]pyridazine core was performed starting from **10a** (Table 1). Replacement of the 4-tetrahydropyranyl group in **10a** with various sizes of aromatic or aliphatic groups revealed that small aliphatic substituents were optimal for VEGFR2 kinase inhibition. The cyclohexyl derivative **10b** (IC_{50} = 11 nM) was about four-fold less active than **10a**, while the thienyl (**10c**, IC_{50} = 19 nM) and (trifluoromethyl)phenyl (**10d**, IC_{50} = 160 nM; **10e**, IC_{50} = 120 nM) compounds exhibited even low

Table 2Effect of the amide substituent R² on VEGFR2 kinase inhibitory activity^a


Compound	R ²	VEGFR2 IC ₅₀ (nM)	Compound	R ²	VEGFR2 IC ₅₀ (nM)
10f		1.0 (0.96–1.1)	16		1.3 (1.2–1.5)
11		12 (11–14)	17		0.96 (0.81–1.1)
12		650 (550–750)	18		25 (19–33)
13		1.3 (1.2–1.5)	19		1.4 (1.3–1.5)
14		1.3 (1.2–1.3)	20		1.2 (1.2–1.3)
15		1.4 (1.2–1.8)	21		3.7 (3.3–4.2)

^a Numbers in parentheses represent 95% confidence interval.**Table 3**Effect of the central phenyl substituent X on VEGFR2 kinase activity and HUVEC growth^a


Compound	X	VEGFR2 IC ₅₀ (nM)	HUVEC ^b IC ₅₀ (nM)
19	H	1.4 (1.3–1.5)	1.7 (0.66–3.8)
23a (TAK-593)	2-Me	0.95 (0.82–1.1)	0.30 (0.28–0.32)
23b	4-Me	1.8 (1.5–2.1)	11 (6.8–17)
23c	6-Me	4.7 (4.2–5.3)	97 (73–130)
23d	2-Et	5.1 (4.2–6.2)	93 (66–130)
23e	2-F	1.1 (1.0–1.3)	0.56 (0.14–1.5)
23f	2-Cl	1.3 (1.1–1.5)	3.0 (1.4–5.8)

^a Numbers in parentheses represent 95% confidence interval.^b Inhibition of VEGF-stimulated HUVEC proliferation.

potency. These results implied that the binding pocket of VEGFR2 for R¹ is rather small. This was supported by the fact that compounds having a cyclopropyl (**10f**, IC₅₀ = 1.0 nM) or methyl (**10g**, IC₅₀ = 1.1 nM) group were more potent than **10b**. Considering these results, we selected the cyclopropyl group as the R¹ substituent for further study.

Next, we examined the effect of amide substituents at the *meta* position of the 6-phenoxy moiety (R², Table 2). In contrast to the results of R¹, the small aliphatic substituents seemed to be less preferable as the R² group. Replacement of the fluorophenyl group in **10f** with a

cyclopropyl group (**11**) resulted in a 12-fold reduction in inhibitory activity against VEGFR2 kinase (IC₅₀ = 12 nM), and the compound with a *tert*-butyl group (**12**) had a 650-fold loss of potency (IC₅₀ = 650 nM). These results suggested that large planar substituents might have a better fit with the VEGFR2 protein. Indeed, except for **18**, the aromatic amide derivatives **10f**, **13–17**, and **19–21** more potently inhibited VEGFR2 kinase than the aliphatic amide derivatives **11** and **12**. No clear difference in activity was observed among the aromatic compounds **10f**, **13–17**, and **19–21**. For example, the fluorophenyl (**10f**), pyridyl (**13**), and isoxazolyl (**14**) derivatives had similarly strong activity against VEGFR2 kinase, although the ring size and number of heteroatoms differed between them. The methylisoxazolyl (**15**) and methyltriazolyl (**16**) compounds also showed similar inhibition of enzymatic activity with IC₅₀ values around 1 nM, indicating that mono-methyl substitution on the heteroaryl did not affect VEGFR2 kinase inhibition. Conversely, the isoxazole **18** possessing two methyl groups at the *ortho* position of the carbonyl group was found to be about 20-fold less active (IC₅₀ = 25 nM) than the dimethylpyrazole derivatives **17** and **19** (IC₅₀ = 0.96, 1.4 nM) which had different substitution patterns. Regarding the size of substituents on the heteroaryl group, even replacement of the 1-methyl group of the pyrazole in **19** with a much larger phenyl group (**20**) was acceptable (IC₅₀ = 1.2 nM). Replacement of the 3-methyl group of the pyrazole in **19** with a trifluoromethyl group (**21**) resulted in a slightly decreased potency (IC₅₀ = 3.7 nM). Further evaluation revealed that the heteroaryl derivatives tended to show lower potency against B-raf kinase than the fluorophenyl compound **10f**. For instance, although **10f** moderately inhibited B-raf kinase with an IC₅₀ of 650 nM, the pyrazole derivative **19** did not significantly inhibit B-raf kinase (IC₅₀ > 10,000 nM). Thus, in terms of kinase selectivity, compound **19** was judged to be preferable to compound **10f**. In addition, **19** strongly suppressed the growth of HUVEC with an IC₅₀ of 1.7 nM,

thereby emerging as a new lead compound for the further development of VEGFR2 inhibitors.

The co-crystal structure of **19** in complex with VEGFR2 was solved, and the result is shown in Figure 3. Compound **19** binds to the inactive (DFG-out) conformation of VEGFR2 in the same manner as the so-called type-II kinase inhibitors.²⁴ When **19** is bound to VEGFR2, the N1-nitrogen of the imidazo[1,2-*b*]pyridazine core interacts with the NH proton of Cys919. The CH proton at the 8-position of the core forms a CH···O hydrogen bond with the carbonyl group of Glu917. The 6-phenoxy moiety extends toward the back pocket, accompanied by interaction of the amide proton with Glu885, the amide carbonyl group with Asp1046, and the terminal pyrazole ring with the hydrophobic pocket. As for the amide group at the 2-position of the imidazo[1,2-*b*]pyridazine, the amide proton is involved in hydrogen bonding with the carbonyl group of Cys919, and the cyclopropane moiety is suitably located in the solvent accessible region. In addition, a small hydrophobic pocket was observed around the central phenyl ring, which indicated the possibility of introducing a substituent on the phenyl moiety.

Thus, the effects of substituents on the central phenyl group were investigated as shown in Table 3. Methyl substitution at the 2-position (**23a**) was found to produce potent HUVEC growth inhibition. While the 2-methyl (**23a**, IC₅₀ = 0.95 nM), 4-methyl (**23b**, IC₅₀ = 1.8 nM), and 6-methyl (**23c**, IC₅₀ = 4.7 nM) derivatives showed similar inhibitory activity against VEGFR2 kinase, compound **23a** inhibited growth of HUVEC (IC₅₀ = 0.30 nM) much stronger than **23b** or **23c** (IC₅₀ = 11, 97 nM). Conversely, replacement of the methyl group in **23a** with an ethyl group (**23d**) decreased both the inhibition of VEGFR2 kinase (IC₅₀ = 5.1 nM) and the inhibition of HUVEC growth (IC₅₀ = 93 nM). This SAR is consistent with the crystal structure analysis of **19** with VEGFR2, in which the space for introducing substituents around the central phenyl ring is limited. Further investigation showed that substitution with the electron-withdrawing group at this position was tolerated. In fact, the 2-fluoro (**23e**) and 2-chloro (**23f**) derivatives exhibited IC₅₀ values below 10 nM in both the enzyme activity (VEGFR2 IC₅₀ = 1.1, 1.3 nM) and cell proliferation (HUVEC IC₅₀ = 0.56, 3.0 nM) assays.

During the course of our study, we observed a discrepancy between the enzyme and cell growth inhibition assays. In fact, the initial compound **1** inhibited VEGFR2 enzyme phosphorylation and VEGF-stimulated growth of HUVEC with IC₅₀ values of 7.1 and 650 nM, while the IC₅₀ values for compound **4** were 6.9 and 9.1 nM, respectively. To better understand the reason for this difference, we performed the kinase assay with varying ATP concentrations and preincubation times (Table 4). In the case of compound **1**, an increase of

Table 4

Inhibition of VEGFR2 kinase in various conditions^a

Compound	VEGFR2 IC ₅₀ (nM)			HUVEC ^d IC ₅₀ (nM)
	ATP 10 μM ^b	ATP 1000 μM ^b		
		5 min ^c	60 min ^c	
1	7.1	35 (30–39)	49 (42–57)	650
4	6.9	10 (9.9–11)	1.1 (1.0–1.1)	9.1
19	1.4	1.8 (1.5–2.1)	0.19 (0.17–0.22)	1.7
23a	0.95	1.1 (1.0–1.1)	0.093 (0.087–0.098)	0.30

^a Numbers in parentheses represent 95% confidence interval.

^b Concentration of ATP.

^c Preincubation time.

^d Inhibition of VEGF-stimulated HUVEC proliferation.

ATP concentration from 10 to 1000 μM resulted in a fivefold increase of the IC₅₀ value (7.1 → 35 nM). On the other hand, the IC₅₀ values for **4** were approximately the same (6.9 → 10 nM). More interestingly, increasing the preincubation time from 5 to 60 min led to an approximate 10-fold decrease in IC₅₀ for **4** (10 → 1.1 nM). This time dependency indicated that compound **4** is a slow-binding inhibitor of VEGFR2. In contrast, compound **1** did not exhibit an increase in activity after preincubation for 60 min, suggesting that it is a fast-binding inhibitor. The enzyme inhibition produced with the longer preincubation time was found to be better correlated with the inhibition of cell proliferation. The VEGFR2 IC₅₀ value obtained with 60-min preincubation for compound **4** was about 50-fold lower than that for **1** (1.1 vs 49 nM), which roughly corresponds to the ratio of IC₅₀ values observed in the HUVEC proliferation assay (9.1 vs 650 nM).

We also evaluated the time dependency of compounds **19** and **23a**, which were again found to be slow-binding inhibitors. After preincubation for 60 min, compounds **19** and **23a** inhibited VEGFR2 kinase with IC₅₀ values of 0.19 and 0.093 nM, respectively. A typical inhibition curve, exemplified by **23a**, is shown in Figure 4. Due to their strong inhibition of the kinase, compounds **19** and **23a** also exhibited significant inhibitory activity in the cell growth assay. Recently, we showed that **23a** has a long residence time on VEGFR2.²⁵ The slow dissociation kinetics of **23a** might contribute to its strong inhibitory potency on HUVEC growth.

The pharmacokinetic properties of selected compounds that showed strong inhibition of HUVEC growth (**19** and **23a,e**) were evaluated in mice (Table 5). It was found that the presence of a substituent at the 2-position is important for increasing the area under the plasma concentration–time curve (AUC) values. After oral administration of compound **19** (10 mg/kg) to mice, an AUC_{0–8h} value of 0.73 μg·h/mL was observed. In contrast, introduc-

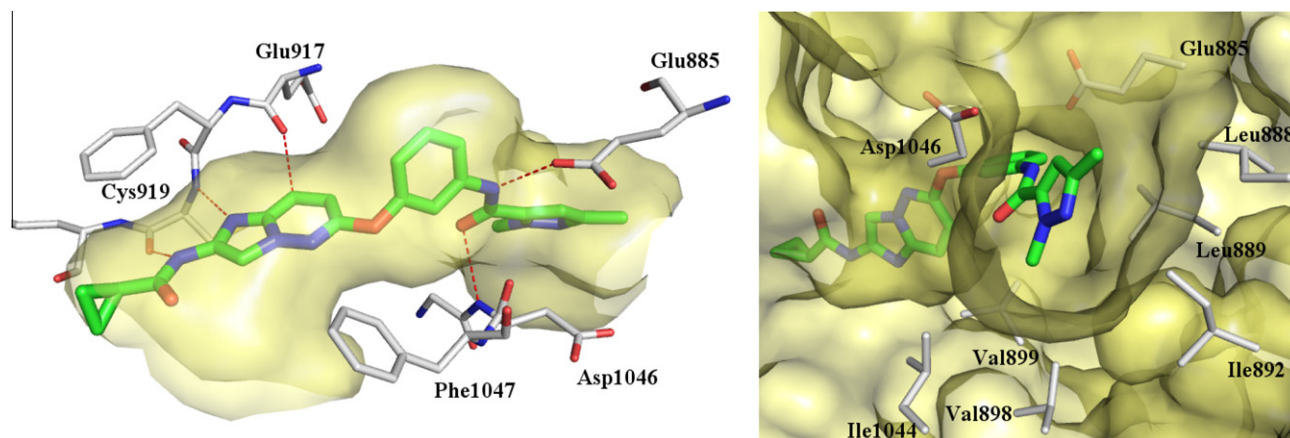


Figure 3. Crystal structure of **19** in complex with VEGFR2 (PDB 3VO3). Dashed lines represent hydrogen bonds.

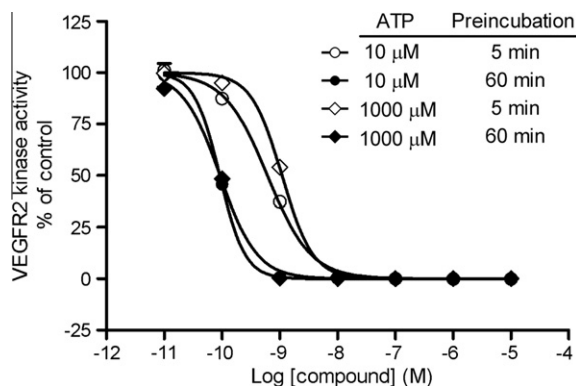


Figure 4. VEGFR2 inhibition curves for **23a** in various conditions. Data represent the mean \pm SD ($n = 4$).

tion of methyl (**23a**) and fluoro (**23e**) groups dramatically increased AUC values (15 and 7.6 $\mu\text{g}\cdot\text{h}/\text{mL}$). We supposed that these higher AUC values were attributed to the improved solubility of **23a** and **23e** compared to **19** in Japanese Pharmacopoeia disintegration test solution 2 (pH 6.8) containing a bile acid (Table 5).

To clarify the effect of the 2-substituents on solubility, $\log D$ values and melting points of **19** and **23a,e** were measured, since general solubility equations include both lipophilicity and melting point.²⁶ The results revealed that there is a relationship between their solubilities and melting points (Table 5). Compound **23a**, which showed the lowest melting point (223 $^{\circ}\text{C}$), was the most soluble (38 $\mu\text{g}/\text{mL}$), while **19** showed the highest melting point (266 $^{\circ}\text{C}$) and the lowest solubility (3.7 $\mu\text{g}/\text{mL}$). The $\log D$ values at pH 7.4 of **19** and **23a,e** were nearly identical. There are similar examples of this relationship in the literature,²⁷ and the authors of this previous report concluded that disruption of molecular planarity by introduction of a substituent resulted in a decreased crystal packing energy and a lower melting point, leading to improved solubility. Thus, the methyl group of **23a** and the fluoro group of **23e** may contribute to distortion of the planar conformation of the test compounds.

Table 5
Pharmacokinetic and physicochemical profiles of **19** and **23a,e**

Compound	Mouse PK ^a		Metabolic stability ^d		Solubility ^e JP2 + BA ($\mu\text{g}/\text{mL}$)	Mp ^f ($^{\circ}\text{C}$)	$\log D_{7.4}$
	AUC _{0–8h} ^b ($\mu\text{g}\cdot\text{h}/\text{mL}$)	C _{8h} ^c ($\mu\text{g}/\text{mL}$)	Human ($\mu\text{L}/\text{min}/\text{mg}$)	Mouse ($\mu\text{L}/\text{min}/\text{mg}$)			
19	0.73	0.053	6	43	3.7	266	2.28
23a	15	0.60	2	31	38	223	2.24
23e	7.6	0.30	9	54	14	234	2.21

^a Compounds (10 mg/kg) were orally administered by cassette dosing.

^b Area under plasma concentration–time curve from 0 to 8 h.

^c Plasma concentration at 8 h after administration.

^d Metabolic stability in hepatic microsomes.

^e Thermodynamic solubility in Japanese Pharmacopoeia disintegration test solution 2 (pH 6.8) containing a bile acid.

^f Determined by differential scanning calorimetry.

Table 6
Pharmacokinetic parameters of **23a** in rats and cynomolgus monkeys^a

Species	iv (0.25 mg/kg)			po (0.5 mg/kg)				BA (%)
	AUC ^b ($\mu\text{g}\cdot\text{h}/\text{mL}$)	V _{dss} (mL/kg)	CL _{tot} (mL/h/kg)	C _{max} ($\mu\text{g}/\text{mL}$)	T _{max} (h)	AUC ^b ($\mu\text{g}\cdot\text{h}/\text{mL}$)	MRT (h)	
Rat	0.571 \pm 0.009	471 \pm 85	438 \pm 7	0.056 \pm 0.012	1.3 \pm 0.6	0.226 \pm 0.092	3.3 \pm 0.8	19.8 \pm 8.1
Monkey	1.313 \pm 0.064	1028 \pm 109	191 \pm 9	0.129 \pm 0.011	2.8 \pm 1.5	1.511 \pm 0.100	11.0 \pm 1.4	57.6 \pm 2.1

^a Pharmacokinetic parameters were obtained by discrete dosing. Data represent mean values \pm SD (rat, $n = 3$; monkey, $n = 4$).

^b Area under plasma concentration–time curve: rat, AUC_{0–24h}; monkey, AUC_{0–48h}.

The methyl derivative **23a**, which showed the largest AUC value, was selected for further evaluation. Compound **23a** was still detected in plasma even when measured 8 h after administration (C_{8h} = 0.60 $\mu\text{g}/\text{mL}$) reflecting its high stability in mouse hepatic microsomes (CL = 31 $\mu\text{L}/\text{min}/\text{mg}$). Since **23a** showed high stability in human hepatic microsomes (CL = 2 $\mu\text{L}/\text{min}/\text{mg}$), it would be expected to have sufficient oral bioavailability in humans.

Pharmacokinetic parameters of **23a** were measured in rats and cynomolgus monkeys (Table 6). After intravenous administration (0.25 mg/kg), **23a** exhibited low plasma clearance (191–438 mL/h/kg) and low to moderate volume of distribution (471–1028 mL/kg) in these species. Oral administration (0.5 mg/kg) to monkeys showed a peak plasma concentration of 0.129 $\mu\text{g}/\text{mL}$ at 2.8 h, and the plasma concentration decreased slowly with a mean residence time of 11.0 h. The AUC_{0–48h} value was 1.511 $\mu\text{g}\cdot\text{h}/\text{mL}$, and the oral bioavailability was 57.6%. These data also predicted desirable pharmacokinetic profiles in humans.

Compound **23a** was examined for its selectivity against a panel of over 260 kinases.²⁵ It showed potent inhibitory activity against VEGFR (VEGFR1–3: IC₅₀ = 3.2, 0.95, 1.1 nM) and PDGFR (PDGFR α , β : IC₅₀ = 4.3, 13 nM) families. Against other kinases, the IC₅₀ values of **23a** were above 100 nM, except for Fms (IC₅₀ = 10 nM) and Ret (IC₅₀ = 18 nM) kinases. Thus, **23a** proved to be a potent VEGFR and PDGFR kinase inhibitor with high selectivity within the human kinome.

We evaluated the antitumor efficacy of **23a** in a nude mouse xenograft model using A549 human lung adenocarcinoma epithelial cells (Fig. 5).²⁸ Tumor growth inhibition was calculated as treatment over control (T/C) values, measured as the increase in treated tumor volumes divided by the increase in control tumor volumes. Consistent with its potent in vitro activity and good oral exposure levels, **23a** showed significant antitumor activity. Upon oral administration of **23a** twice daily at doses of 0.25, 1, and 4 mg/kg for 2 weeks, the T/C values were 34, 8, and –8%, respectively. No obvious weight loss or morbidity was observed over the entire treatment period.

We then studied the pharmacokinetic and pharmacodynamic properties of **23a**, to gain insight into its potent antitumor activity (Fig. 6).²⁸ Oral administration of **23a** at 1 mg/kg to athymic nude mice showed that the concentration of **23a** in plasma (0.451 $\mu\text{g}/$

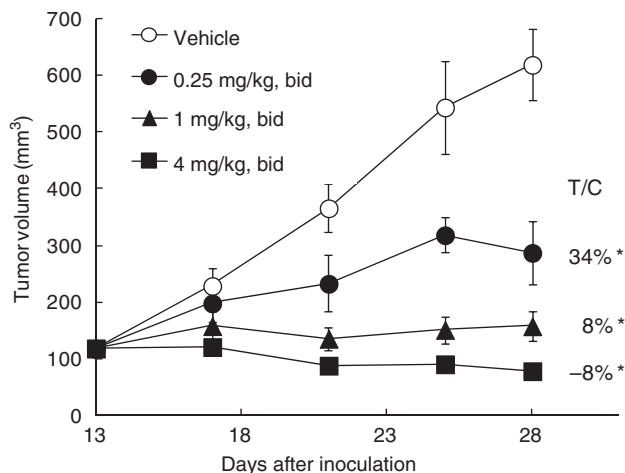


Figure 5. Antitumor efficacy of **23a** in an A549 xenograft mouse model. A549 tumor-bearing nude mice were orally administered **23a** (0.25, 1, and 4 mg/kg) twice daily for 14 days (day 14–27). Data represent mean \pm SD ($n = 5$). * $p \leq 0.025$ versus vehicle control as determined by a one-tailed Williams' test. Antitumor effects are expressed as T/C values (increase in treated tumor volume/increase in control tumor volume) $\times 100$.

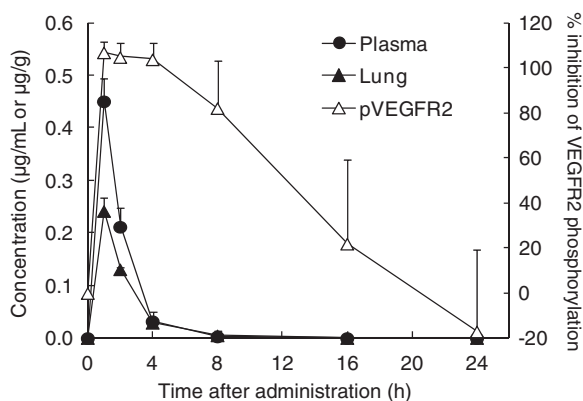


Figure 6. PK/PD analysis of **23a**. Nude mice ($n = 3$) were orally administered **23a** (1 mg/kg), and the concentration of **23a** in plasma and lung tissue was determined by LC/MS/MS. For PD analysis, nude mice ($n = 4$) were treated with an oral dose of **23a** (1 mg/kg), and the lung tissue was collected 5 min after VEGF (20 µg/mouse) injection. VEGFR2 phosphorylation in the lung tissue was assessed by Western blot.

mL) and lung tissue (0.242 µg/g) at 1 h after dosing had achieved levels sufficient to inhibit VEGFR2 kinase. At 8 h after dosing, the concentration of **23a** was below or near the detectable limit in either plasma (<0.003 µg/mL) or lung tissue (<0.015 µg/g). On the other hand, phospho-VEGFR2 in lung tissue was almost completely suppressed at not only 1 h, but also 8 h after oral administration of **23a**, and restored to baseline after 16 h. Compound **23a** has a long-lasting inhibitory effect on VEGFR2 kinase,²⁵ which might contribute to in vivo efficacy.²⁹ Consequently, we speculated that the potent in vivo efficacy of **23a** was achieved by a combination of its favorable pharmacokinetic profile and its long residence time on VEGFR2.

4. Conclusion

To discover potent VEGFR2 kinase inhibitors with strong in vivo antitumor efficacy, we designed and synthesized 2-acylamino-6-phenoxyimidazo[1,2-*b*]pyridazine derivatives, which were a hybrid of 6-phenoxyimidazo[1,2-*b*]pyridazine **1** and 2-acylaminoimidazo[1,2-*b*]pyridazine **2**. These efforts led to a significant enhancement of cell growth inhibition. Optimization of the amide

substituents at the 2-position showed that small aliphatic groups were suitable to maintain inhibitory activity. The heteroaryl groups were suitable for the amide substituent at the *meta* position of the 6-phenoxy moiety. Furthermore, the introduction of a methyl group on the central phenyl ring resulted in the discovery of **23a**, the compound possessing the strongest potency in the cell-based assay and favorable pharmacokinetic properties based on its improved solubility. Compound **23a** showed potent activity against PDGFR kinases as well as VEGFR kinases with high kinase selectivity. It exhibited potent antitumor efficacy in an A549 xenograft mouse model. Ultimately, **23a** (TAK-593) was selected as a clinical candidate for the treatment of human cancer.

5. Experimental section

5.1. Chemistry

Commercial reagents and solvents were used without additional purification. Microwave assisted reactions were carried out in a Biotage Initiator microwave reactor. Reaction progress was determined by thin layer chromatography (TLC) on Silica Gel 60 F254 plates (Merck) or NH TLC plates (Fuji Silysia). Column chromatography was carried out using a Purif Purification System (Moritex) with silica gel (Purif-Pack SI-60, Fuji Silysia) or basic silica gel (Purif-Pack NH-60, Fuji Silysia) cartridges. Melting points were determined on a Yanagimoto micro melting point, BÜCHI Melting Point B-545, or OptiMelt melting point apparatus and were not corrected. Proton nuclear magnetic resonance (¹H NMR) spectra were recorded on a Bruker DPX 300 (300 MHz), Varian Mercury 300 (300 MHz), or Bruker AV 400 (400 MHz) instrument. Chemical shifts (δ) are reported in ppm relative to internal tetramethylsilane. Peak multiplicities are expressed as follows: s, singlet; d, doublet; t, triplet; q, quartet; dd, doublet of doublet; dt, doublet of triplet; td, triplet of doublet; ddd, doublet of doublet of doublet; m, multiplet; br s, broad singlet. Coupling constants (*J*) are given in hertz (Hz). Elemental analyses and high resolution mass spectrometry (HRMS) were performed at the Takeda Analytical Research Laboratories, Ltd. Abbreviations are used as follows: DMA, *N,N*-dimethylacetamide; DMF, *N,N*-dimethylformamide; DMSO, dimethyl sulfoxide; EDC-HCl, 1-ethyl-3-[3-(dimethylamino)propyl]carbodiimide hydrochloride; HOBt, 1-hydroxybenzotriazole; NMP, *N*-methylpyrrolidone; THF, tetrahydrofuran.

5.1.1. Ethyl (6-iodoimidazo[1,2-*b*]pyridazin-2-yl)carbamate (**6**)

To a stirred solution of 3-amino-6-iodopyridazine (**5**)³⁰ (27.0 g, 122 mmol) in DMA (270 mL) were added ethyl (chloroacetyl)carbamate (32.4 g, 196 mmol) and Na₂HPO₄ (43.4 g, 306 mmol), and the mixture was stirred at 110 °C for 3 h. After cooling to room temperature, the mixture was diluted with water (810 mL), and the precipitate was collected by filtration and washed with CH₃CN followed by Et₂O to give **6** (33.0 g, 81%) as a dark brown solid. ¹H NMR (300 MHz, DMSO-*d*₆) δ 1.26 (3H, t, *J* = 7.1 Hz), 4.17 (2H, q, *J* = 7.1 Hz), 7.47 (1H, d, *J* = 9.2 Hz), 7.70 (1H, d, *J* = 9.2 Hz), 8.06 (1H, s), 10.51 (1H, br s).

5.1.2. 6-Iodoimidazo[1,2-*b*]pyridazin-2-amine (**7**)

A suspension of Ba(OH)₂·8H₂O (14.5 g, 46.0 mmol) in water (240 mL) was stirred at 80 °C for 15 min. To the mixture was added a solution of **6** (10.2 g, 30.7 mmol) in NMP (80 mL), and the mixture was stirred at 120 °C for 8 h. After cooling to room temperature, the mixture was diluted with water (480 mL) and stirred for 1 h. The mixture was extracted with EtOAc/THF, and the organic layer was washed with brine, dried over MgSO₄, and filtered. The filtrate was concentrated in vacuo, and the residue was triturated with *i*-Pr₂O to give **7** (6.10 g, 76%) as a brown solid. ¹H NMR

(300 MHz, DMSO- d_6) δ 5.61 (2H, s), 7.22 (1H, d, J = 8.7 Hz), 7.36 (1H, s), 7.39 (1H, d, J = 8.7 Hz).

5.1.3. *N*-(6-Iodoimidazo[1,2-*b*]pyridazin-2-yl)cyclopropanecarboxamide (8f)

To a stirred solution of **7** (1.00 g, 3.85 mmol) in DMA (10 mL) was added cyclopropanecarbonyl chloride (384 μ L, 4.23 mmol), and the mixture was stirred at room temperature for 4 h. The mixture was diluted with water and extracted with EtOAc/THF (2:1). The organic layer was washed with brine, dried over $MgSO_4$, and filtered. The filtrate was concentrated in vacuo, and the residue was triturated with *n*-hexane/EtOAc (4:1) to give **8f** (1.01 g, 80%) as a dark brown solid. 1H NMR (300 MHz, DMSO- d_6) δ 0.82–0.86 (4H, m), 1.90–2.00 (1H, m), 7.49 (1H, d, J = 9.3 Hz), 7.73 (1H, d, J = 9.3 Hz), 8.23 (1H, s), 11.20 (1H, s).

Compounds **8a–e,g** were prepared from **7** and the appropriate acyl chloride in a manner similar to that described for **8f**.

5.1.4. *N*-(6-Iodoimidazo[1,2-*b*]pyridazin-2-yl)tetrahydro-2H-pyran-4-carboxamide (8a)

Yield 73%, light brown solid. 1H NMR (300 MHz, DMSO- d_6) δ 1.54–1.76 (4H, m), 2.66–2.80 (1H, m), 3.27–3.40 (2H, m), 3.84–3.96 (2H, m), 7.49 (1H, d, J = 9.3 Hz), 7.74 (1H, d, J = 9.3 Hz), 8.28 (1H, s), 10.91 (1H, s).

5.1.5. *N*-(6-Iodoimidazo[1,2-*b*]pyridazin-2-yl)cyclohexanecarboxamide (8b)

Yield 50%, white solid. 1H NMR (300 MHz, DMSO- d_6) δ 1.12–1.49 (6H, m), 1.59–1.85 (5H, m), 7.48 (1H, d, J = 9.3 Hz), 7.73 (1H, d, J = 9.3 Hz), 8.22–8.31 (1H, m), 10.80 (1H, s).

5.1.6. *N*-(6-Iodoimidazo[1,2-*b*]pyridazin-2-yl)-3-methylthiophene-2-carboxamide (8c)

Yield 61%, pale yellow solid. 1H NMR (400 MHz, DMSO- d_6) δ 2.47–2.50 (3H, m), 7.03 (1H, d, J = 4.9 Hz), 7.53 (1H, d, J = 9.4 Hz), 7.69 (1H, d, J = 4.9 Hz), 7.77 (1H, d, J = 9.2 Hz), 8.40 (1H, s), 10.96 (1H, s).

5.1.7. *N*-(6-Iodoimidazo[1,2-*b*]pyridazin-2-yl)-3-(trifluoromethyl)benzamide (8d)

Yield 63%, white solid. 1H NMR (300 MHz, DMSO- d_6) δ 7.55 (1H, d, J = 9.3 Hz), 7.74–7.85 (2H, m), 7.98 (1H, d, J = 7.8 Hz), 8.37 (1H, d, J = 7.7 Hz), 8.46 (1H, s), 8.51 (1H, s), 11.77 (1H, s).

5.1.8. *N*-(6-Iodoimidazo[1,2-*b*]pyridazin-2-yl)-4-(trifluoromethyl)benzamide (8e)

Yield 49%, white solid. 1H NMR (300 MHz, DMSO- d_6) δ 7.55 (1H, d, J = 9.3 Hz), 7.81 (1H, d, J = 9.3 Hz), 7.91 (2H, d, J = 8.3 Hz), 8.26 (2H, d, J = 8.1 Hz), 8.51 (1H, s), 11.72 (1H, s).

5.1.9. *N*-(6-Iodoimidazo[1,2-*b*]pyridazin-2-yl)acetamide (8g)

Yield 43%, white solid. 1H NMR (300 MHz, DMSO- d_6) δ 2.09 (3H, s), 7.49 (1H, d, J = 9.3 Hz), 7.74 (1H, d, J = 9.3 Hz), 8.25 (1H, s), 10.91 (1H, s).

5.1.10. *N*-[6-(3-Aminophenoxy)imidazo[1,2-*b*]pyridazin-2-yl]cyclopropanecarboxamide (9f)

A mixture of **8f** (805 mg, 2.45 mmol), 3-aminophenol (430 mg, 3.94 mmol), and K_2CO_3 (847 mg, 6.13 mmol) in DMF (6 mL) was stirred at 180 °C for 30 min using a microwave synthesizer. The mixture was concentrated in vacuo. The residue was diluted with water and extracted with EtOAc/THF (1:1). The organic layer was washed with brine, dried over Na_2SO_4 , and filtered. The filtrate was concentrated in vacuo, and the residue was purified by silica gel column chromatography (*n*-hexane/EtOAc 70:30 to 0:100) to

give **9f** (468 mg, 62%) as a brown solid. 1H NMR (300 MHz, DMSO- d_6) δ 0.75–0.85 (4H, m), 1.87–1.97 (1H, m), 5.31 (2H, s), 6.27–6.32 (1H, m), 6.35 (1H, t, J = 2.2 Hz), 6.40–6.46 (1H, m), 6.95 (1H, d, J = 9.5 Hz), 7.05 (1H, t, J = 8.0 Hz), 7.98 (1H, s), 8.00 (1H, d, J = 9.5 Hz), 11.08 (1H, s).

Compounds **9a–e,g** were prepared from the corresponding iodides **8a–e,g** in a manner similar to that described for **9f**.

5.1.11. *N*-[6-(3-Aminophenoxy)imidazo[1,2-*b*]pyridazin-2-yl]tetrahydro-2H-pyran-4-carboxamide (9a)

Yield 42%, white solid. 1H NMR (300 MHz, DMSO- d_6) δ 1.57–1.73 (4H, m), 2.64–2.77 (1H, m), 3.26–3.39 (2H, m), 3.84–3.94 (2H, m), 5.30 (2H, s), 6.27–6.45 (3H, m), 6.95 (1H, d, J = 9.6 Hz), 7.05 (1H, t, J = 8.1 Hz), 7.97–8.03 (2H, m), 10.78 (1H, s).

5.1.12. *N*-[6-(3-Aminophenoxy)imidazo[1,2-*b*]pyridazin-2-yl]cyclohexanecarboxamide (9b)

Yield 51%, colorless oil. 1H NMR (400 MHz, $CDCl_3$) δ 1.21–1.37 (2H, m), 1.45–1.59 (2H, m), 1.65–2.02 (6H, m), 2.21–2.34 (1H, m), 3.77 (2H, br s), 6.50 (1H, t, J = 2.1 Hz), 6.52–6.57 (2H, m), 6.81 (1H, d, J = 9.6 Hz), 7.17 (1H, t, J = 8.0 Hz), 7.70 (1H, d, J = 9.6 Hz), 8.01–8.14 (1H, m), 8.22 (1H, s).

5.1.13. *N*-[6-(3-Aminophenoxy)imidazo[1,2-*b*]pyridazin-2-yl]-3-methylthiophene-2-carboxamide (9c)

Yield 58%, pale yellow solid. 1H NMR (400 MHz, $CDCl_3$) δ 2.62 (3H, s), 3.78 (2H, br s), 6.52 (1H, t, J = 2.1 Hz), 6.56 (2H, dd, J = 8.1, 2.0 Hz), 6.83 (1H, d, J = 9.5 Hz), 6.95 (1H, d, J = 4.9 Hz), 7.18 (1H, t, J = 8.1 Hz), 7.37 (1H, d, J = 5.1 Hz), 7.67 (1H, dd, J = 9.5, 1.7 Hz), 8.32 (1H, s), 8.36 (1H, br s).

5.1.14. *N*-[6-(3-Aminophenoxy)imidazo[1,2-*b*]pyridazin-2-yl]-3-(trifluoromethyl)benzamide (9d)

Yield 54%, white solid. 1H NMR (400 MHz, $CDCl_3$) δ 3.80 (2H, br s), 6.53 (1H, t, J = 2.1 Hz), 6.55–6.60 (2H, m), 6.84 (1H, d, J = 9.5 Hz), 7.20 (1H, t, J = 8.0 Hz), 7.58 (1H, d, J = 9.5 Hz), 7.64 (1H, t, J = 7.8 Hz), 7.82 (1H, d, J = 7.8 Hz), 8.11 (1H, d, J = 7.8 Hz), 8.21 (1H, s), 8.39 (1H, s), 9.16 (1H, br s).

5.1.15. *N*-[6-(3-Aminophenoxy)imidazo[1,2-*b*]pyridazin-2-yl]-4-(trifluoromethyl)benzamide (9e)

Yield 44%, white solid. 1H NMR (400 MHz, $CDCl_3$) δ 3.80 (2H, br s), 6.53 (1H, t, J = 2.2 Hz), 6.55–6.60 (2H, m), 6.83 (1H, d, J = 9.6 Hz), 7.20 (1H, t, J = 8.0 Hz), 7.54 (1H, d, J = 9.6 Hz), 7.76 (2H, d, J = 8.5 Hz), 8.04 (2H, d, J = 8.3 Hz), 8.39 (1H, s), 9.13 (1H, s).

5.1.16. *N*-[6-(3-Aminophenoxy)imidazo[1,2-*b*]pyridazin-2-yl]acetamide (9g)

Yield 72%, white solid. 1H NMR (400 MHz, DMSO- d_6) δ 2.07 (3H, s), 5.31 (2H, br s), 6.30 (1H, dd, J = 7.9, 1.6 Hz), 6.36 (1H, t, J = 2.2 Hz), 6.43 (1H, dd, J = 8.1, 1.2 Hz), 6.96 (1H, d, J = 9.8 Hz), 7.05 (1H, t, J = 8.1 Hz), 7.97–8.01 (2H, m), 10.79 (1H, s).

5.1.17. *N*-[3-({2-[(Cyclopropylcarbonyl)amino]imidazo[1,2-*b*]pyridazin-6-yl}oxy)phenyl]-3-fluorobenzamide (10f)

To a stirred solution of **9f** (100 mg, 0.32 mmol) in DMA (3 mL) was added 3-fluorobenzoyl chloride (43 μ L, 0.36 mmol), and the mixture was stirred at room temperature overnight. The mixture was diluted with water and extracted with EtOAc. The organic layer was washed with water and brine, dried over $MgSO_4$, and filtered. The filtrate was concentrated in vacuo, and the residue was purified by basic silica gel column chromatography (*n*-hexane/EtOAc 100:0 to 0:100) to give **10f** (56 mg, 40%) as a white solid. Mp 263–264 °C. 1H NMR (300 MHz, DMSO- d_6) δ 0.76–0.85 (4H, m), 1.87–1.98 (1H, m), 7.02 (1H, dd, J = 8.1, 2.2 Hz), 7.07 (1H, d, J = 9.5 Hz), 7.41–7.49

(2H, m), 7.54–7.83 (5H, m), 7.98 (1H, s), 8.06 (1H, d, $J = 9.5$ Hz), 10.43 (1H, s), 11.08 (1H, s). Anal. Calcd for $C_{23}H_{18}FN_5O_3$: C, 64.03; H, 4.21; N, 16.23. Found: C, 63.76; H, 4.12; N, 16.10.

Compounds **10a–e.g** were prepared from the corresponding anilines **9a–e.g** in a manner similar to that described for **10f**.

5.1.18. *N*-[6-(3-[(3-Fluorophenyl)carbonyl]amino)phenoxy]imidazo[1,2-*b*]pyridazin-2-yl]tetrahydro-2H-pyran-4-carboxamide (10a)

Yield 34%, white solid. Mp 230–231 °C. 1H NMR (400 MHz, DMSO- d_6) δ 1.58–1.74 (4H, m), 2.65–2.76 (1H, m), 3.28–3.37 (2H, m), 3.86–3.92 (2H, m), 7.02 (1H, dd, $J = 8.1, 1.5$ Hz), 7.08 (1H, d, $J = 9.5$ Hz), 7.42–7.49 (2H, m), 7.56–7.62 (1H, m), 7.64–7.68 (1H, m), 7.72–7.78 (2H, m), 7.80 (1H, d, $J = 7.8$ Hz), 8.03 (1H, s), 8.06 (1H, d, $J = 9.5$ Hz), 10.45 (1H, s), 10.81 (1H, s). Anal. Calcd for $C_{25}H_{22}FN_5O_4 \cdot 0.25H_2O$: C, 62.56; H, 4.72; N, 14.59. Found: C, 62.64; H, 4.63; N, 14.82.

5.1.19. *N*-[3-(2-[(Cyclohexylcarbonyl)amino]imidazo[1,2-*b*]pyridazin-6-yl)oxy)phenyl]-3-fluorobenzamide (10b)

Yield 54%, white solid. Mp 216–217 °C. 1H NMR (300 MHz, DMSO- d_6) δ 1.09–1.49 (5H, m), 1.57–1.84 (5H, m), 2.39–2.48 (1H, m), 6.98–7.10 (2H, m), 7.40–7.50 (2H, m), 7.54–7.69 (2H, m), 7.71–7.83 (3H, m), 8.00–8.08 (2H, m), 10.44 (1H, s), 10.69 (1H, s). Anal. Calcd for $C_{26}H_{24}FN_5O_3 \cdot 0.2H_2O$: C, 65.45; H, 5.15; N, 14.68. Found: C, 65.49; H, 5.21; N, 14.63.

5.1.20. *N*-[6-(3-[(3-Fluorophenyl)carbonyl]amino)phenoxy]imidazo[1,2-*b*]pyridazin-2-yl]-3-methylthiophene-2-carboxamide (10c)

Yield 33%, white solid. Mp 203–204 °C. 1H NMR (300 MHz, DMSO- d_6) δ 2.47 (3H, s), 6.99–7.07 (2H, m), 7.12 (1H, d, $J = 9.5$ Hz), 7.41–7.50 (2H, m), 7.55–7.70 (3H, m), 7.73–7.85 (3H, m), 8.01–8.18 (2H, m), 10.45 (1H, s), 10.86 (1H, s). HRMS–ESI (m/z): $[M+H]^+$ calcd for $C_{25}H_{18}FN_5O_3S$, 488.1187; found, 488.1166.

5.1.21. 3-Fluoro-*N*-(3-[[2-[(3-(trifluoromethyl)phenyl]carbonyl]amino]imidazo[1,2-*b*]pyridazin-6-yl]oxy]phenyl)benzamide (10d)

Yield 52%, amorphous solid. 1H NMR (300 MHz, DMSO- d_6) δ 7.06 (1H, ddd, $J = 8.0, 2.4, 0.9$ Hz), 7.15 (1H, d, $J = 9.8$ Hz), 7.41–7.51 (2H, m), 7.60 (1H, td, $J = 8.0, 6.1$ Hz), 7.66–7.72 (1H, m), 7.74–7.85 (4H, m), 7.97 (1H, d, $J = 7.6$ Hz), 8.10–8.16 (1H, m), 8.25 (1H, s), 8.36 (1H, d, $J = 8.0$ Hz), 8.45 (1H, s), 10.47 (1H, s), 11.68 (1H, s). HRMS–ESI (m/z): $[M+H]^+$ calcd for $C_{27}H_{17}F_4N_5O_3$, 536.1340; found, 536.1327.

5.1.22. 3-Fluoro-*N*-(3-[[2-[(4-(trifluoromethyl)phenyl]carbonyl]amino]imidazo[1,2-*b*]pyridazin-6-yl]oxy]phenyl)benzamide (10e)

Yield 55%, white solid. Mp 211–212 °C. 1H NMR (300 MHz, DMSO- d_6) δ 7.06 (1H, dd, $J = 8.0, 2.2$ Hz), 7.11–7.18 (1H, m), 7.40–7.51 (2H, m), 7.54–7.64 (1H, m), 7.65–7.71 (1H, m), 7.73–7.84 (3H, m), 7.89 (2H, d, $J = 8.4$ Hz), 8.13 (1H, d, $J = 9.5$ Hz), 8.21–8.29 (3H, m), 10.46 (1H, s), 11.61 (1H, s). Anal. Calcd for $C_{27}H_{17}F_4N_5O_3 \cdot 0.5H_2O$: C, 59.56; H, 3.33; N, 12.86. Found: C, 59.75; H, 3.46; N, 12.80.

5.1.23. *N*-(3-[[2-(Acetyl)amino]imidazo[1,2-*b*]pyridazin-6-yl]oxy)phenyl]-3-fluorobenzamide (10g)

Yield 76%, white solid. Mp 304–305 °C. 1H NMR (300 MHz, DMSO- d_6) δ 2.07 (3H, s), 6.99–7.11 (2H, m), 7.39–7.51 (2H, m), 7.53–7.70 (2H, m), 7.71–7.84 (3H, m), 7.97–8.09 (2H, m), 10.44 (1H, s), 10.80 (1H, s). Anal. Calcd for $C_{21}H_{16}FN_5O_3 \cdot 0.2H_2O$: C, 61.67; H, 4.04; N, 17.12. Found: C, 61.94; H, 4.09; N, 16.86.

5.1.24. *N*-[6-(3-[(3-(Trifluoromethyl)phenyl)carbonyl]amino)phenoxy]imidazo[1,2-*b*]pyridazin-2-yl]tetrahydro-2H-pyran-4-carboxamide (4)

To an ice-cooled stirred solution of **9a** (200 mg, 0.57 mmol) in DMA (2 mL) was added 3-(trifluoromethyl)benzoyl chloride (100 μ L, 0.68 mmol), and the mixture was stirred at room temperature for 2 h. The mixture was diluted with aqueous $NaHCO_3$ and extracted with EtOAc. The organic layer was washed with brine, dried over $MgSO_4$ and filtered. The filtrate was concentrated in vacuo, and the residue was purified by silica gel column chromatography (EtOAc/MeOH 100:0 to 95:5) followed by recrystallization from *n*-hexane/EtOAc to give **4** (221 mg, 74%) as a white solid. Mp 205–206 °C. 1H NMR (300 MHz, DMSO- d_6) δ 1.56–1.73 (4H, m), 2.62–2.78 (1H, m), 3.26–3.38 (2H, m), 3.83–3.93 (2H, m), 7.00–7.06 (1H, m), 7.08 (1H, d, $J = 9.6$ Hz), 7.46 (1H, t, $J = 8.1$ Hz), 7.64–7.83 (3H, m), 7.95–7.99 (1H, m), 8.03 (1H, s), 8.06 (1H, d, $J = 9.6$ Hz), 8.23–8.29 (2H, m), 10.60 (1H, s), 10.80 (1H, s). Anal. Calcd for $C_{26}H_{22}F_3N_5O_4 \cdot 0.3H_2O$: C, 58.82; H, 4.29; N, 13.19. Found: C, 58.80; H, 4.36; N, 13.06.

Compounds **11–21** were prepared from **9f** and the appropriate acyl chloride in a manner similar to that described for **10f**.

5.1.25. *N*-[3-(2-[(Cyclopropylcarbonyl)amino]imidazo[1,2-*b*]pyridazin-6-yl)oxy)phenyl]cyclopropanecarboxamide (11)

Yield 70%, white solid. Mp 273–274 °C (*n*-hexane/EtOAc). 1H NMR (300 MHz, DMSO- d_6) δ 0.77–0.82 (8H, m), 1.70–1.78 (1H, m), 1.87–1.97 (1H, m), 6.90 (1H, dt, $J = 6.9, 2.2$ Hz), 7.05 (1H, s), 7.30–7.42 (2H, m), 7.57 (1H, s), 7.96 (1H, s), 8.03 (1H, d, $J = 9.5$ Hz), 10.34 (1H, s), 11.08 (1H, s). Anal. Calcd for $C_{20}H_{19}N_5O_3 \cdot 0.3H_2O$: C, 62.75; H, 5.16; N, 18.30. Found: C, 62.74; H, 5.18; N, 18.00.

5.1.26. *N*-(6-(3-[(2,2-Dimethylpropanoyl)amino]phenoxy]imidazo[1,2-*b*]pyridazin-2-yl)cyclopropanecarboxamide (12)

Yield 60%, white solid. Mp 234–235 °C (*n*-hexane/EtOAc). 1H NMR (400 MHz, $CDCl_3$) δ 0.86–0.93 (2H, m), 1.08–1.14 (2H, m), 1.31 (9H, s), 1.55–1.59 (1H, m), 6.83 (1H, d, $J = 9.5$ Hz), 6.94 (1H, ddd, $J = 8.0, 2.3, 1.0$ Hz), 7.26–7.40 (3H, m), 7.60 (1H, t, $J = 2.2$ Hz), 7.72 (1H, d, $J = 9.5$ Hz), 8.14 (1H, s), 8.46 (1H, s). HRMS–ESI (m/z): $[M+H]^+$ calcd for $C_{21}H_{23}N_5O_3$, 394.1874; found, 394.1857.

5.1.27. *N*-[3-(2-[(Cyclopropylcarbonyl)amino]imidazo[1,2-*b*]pyridazin-6-yl)oxy)phenyl]pyridine-4-carboxamide (13)

Yield 78%, white solid. Mp 257–259 °C (EtOH). 1H NMR (300 MHz, DMSO- d_6) δ 0.75–0.85 (4H, m), 1.84–2.00 (1H, m), 7.01–7.07 (1H, m), 7.08 (1H, d, $J = 9.6$ Hz), 7.46 (1H, t, $J = 8.1$ Hz), 7.63–7.69 (1H, m), 7.73 (1H, t, $J = 2.1$ Hz), 7.82–7.87 (2H, m), 7.98 (1H, s), 8.06 (1H, d, $J = 9.6$ Hz), 8.76–8.81 (2H, m), 10.62 (1H, s), 11.09 (1H, s). Anal. Calcd for $C_{22}H_{18}N_6O_3 \cdot 0.2H_2O$: C, 63.21; H, 4.44; N, 20.10. Found: C, 63.28; H, 4.55; N, 19.97.

5.1.28. *N*-[3-(2-[(Cyclopropylcarbonyl)amino]imidazo[1,2-*b*]pyridazin-6-yl)oxy)phenyl]isoxazole-5-carboxamide (14)

Yield 57%, white solid. Mp 237–239 °C. 1H NMR (300 MHz, DMSO- d_6) δ 0.75–0.85 (4H, m), 1.85–1.99 (1H, m), 7.02–7.10 (2H, m), 7.25 (1H, d, $J = 1.7$ Hz), 7.46 (1H, t, $J = 8.2$ Hz), 7.63–7.72 (2H, m), 7.98 (1H, s), 8.06 (1H, d, $J = 9.4$ Hz), 8.81 (1H, d, $J = 1.7$ Hz), 10.87 (1H, s), 11.08 (1H, s). Anal. Calcd for $C_{20}H_{16}N_6O_4$: C, 59.40; H, 3.99; N, 20.78. Found: C, 59.09; H, 3.97; N, 20.73.

5.1.29. *N*-[3-(2-[(Cyclopropylcarbonyl)amino]imidazo[1,2-*b*]pyridazin-6-yl)oxy)phenyl]-3-methylisoxazole-5-carboxamide (15)

Yield 22%, white solid. Mp 241–243 °C (*n*-hexane/EtOAc). 1H NMR (300 MHz, DMSO- d_6) δ 0.73–0.87 (4H, m), 1.86–1.98 (1H, m), 2.32 (3H, s), 7.01–7.14 (3H, m), 7.45 (1H, t, $J = 8.2$ Hz), 7.62–

7.74 (2H, m), 7.98 (1H, s), 8.06 (1H, d, $J = 9.8$ Hz), 10.82 (1H, s), 11.10 (1H, s). HRMS–ESI (m/z): $[M+H]^+$ calcd for $C_{21}H_{18}N_6O_4$, 419.1462; found, 419.1429.

5.1.30. *N*-[3-({2-[(Cyclopropylcarbonyl)amino]imidazo[1,2-*b*]pyridazin-6-yl}oxy)phenyl]-1-methyl-1*H*-1,2,3-triazole-5-carboxamide (16)

Yield 67%, white solid. Mp 282–284 °C (EtOAc). 1H NMR (300 MHz, DMSO- d_6) δ 0.79–0.82 (4H, m), 1.87–1.96 (1H, m), 4.23 (3H, s), 7.02–7.09 (2H, m), 7.46 (1H, t, $J = 8.1$ Hz), 7.56–7.65 (2H, m), 7.96 (1H, s), 8.05 (1H, d, $J = 9.6$ Hz), 8.37 (1H, s), 10.61 (1H, s), 11.09 (1H, s). Anal. Calcd for $C_{20}H_{18}N_8O_3 \cdot 0.1EtOAc$: C, 57.35; H, 4.44; N, 26.23. Found: C, 57.24; H, 4.58; N, 26.00.

5.1.31. *N*-[3-({2-[(Cyclopropylcarbonyl)amino]imidazo[1,2-*b*]pyridazin-6-yl}oxy)phenyl]-1,5-dimethyl-1*H*-pyrazole-3-carboxamide (17)

Yield 42%, white solid. Mp 226–227 °C (*n*-hexane/EtOAc). 1H NMR (300 MHz, DMSO- d_6) δ 0.78–0.83 (4H, m), 1.88–1.96 (1H, m), 2.30 (3H, s), 3.82 (3H, s), 6.54 (1H, s), 6.91–6.96 (1H, m), 7.05 (1H, d, $J = 9.6$ Hz), 7.37 (1H, t, $J = 8.1$ Hz), 7.69–7.73 (1H, m), 7.76–7.78 (1H, m), 7.97 (1H, s), 8.04 (1H, d, $J = 9.6$ Hz), 10.10 (1H, s), 11.09 (1H, s). Anal. Calcd for $C_{22}H_{21}N_7O_3 \cdot 1.2H_2O$: C, 58.32; H, 5.21; N, 21.64. Found: C, 58.41; H, 5.32; N, 21.36.

5.1.32. *N*-[3-({2-[(Cyclopropylcarbonyl)amino]imidazo[1,2-*b*]pyridazin-6-yl}oxy)phenyl]-3,5-dimethylisoxazole-4-carboxamide (18)

Yield 73%, white solid. Mp 227–228 °C (*n*-hexane/EtOAc). 1H NMR (300 MHz, DMSO- d_6) δ 0.79–0.82 (4H, m), 1.88–1.95 (1H, m), 2.32 (3H, s), 2.54 (3H, s), 6.98–7.02 (1H, m), 7.06 (1H, d, $J = 9.6$ Hz), 7.42 (1H, t, $J = 8.1$ Hz), 7.48–7.51 (1H, m), 7.61–7.64 (1H, m), 7.96 (1H, s), 8.05 (1H, d, $J = 9.6$ Hz), 10.19 (1H, s), 11.09 (1H, s). Anal. Calcd for $C_{22}H_{20}N_6O_4$: C, 61.10; H, 4.66; N, 19.43. Found: C, 60.83; H, 4.74; N, 19.31.

5.1.33. *N*-[3-({2-[(Cyclopropylcarbonyl)amino]imidazo[1,2-*b*]pyridazin-6-yl}oxy)phenyl]-1,3-dimethyl-1*H*-pyrazole-5-carboxamide (19)

Yield 54%, white solid. Mp 266 °C (EtOH/THF). 1H NMR (300 MHz, DMSO- d_6) δ 0.79–0.83 (4H, m), 1.87–1.97 (1H, m), 2.19 (3H, s), 3.98 (3H, s), 6.82 (1H, s), 6.99–7.03 (1H, m), 7.07 (1H, d, $J = 9.6$ Hz), 7.43 (1H, t, $J = 8.1$ Hz), 7.60–7.64 (1H, m), 7.65–7.68 (1H, m), 7.97 (1H, s), 8.06 (1H, d, $J = 9.6$ Hz), 10.24 (1H, s), 11.10 (1H, s). Anal. Calcd for $C_{22}H_{21}N_7O_3 \cdot 0.2EtOH$: C, 61.05; H, 5.08; N, 22.25. Found: C, 61.03; H, 5.04; N, 22.24.

5.1.34. *N*-[3-({2-[(Cyclopropylcarbonyl)amino]imidazo[1,2-*b*]pyridazin-6-yl}oxy)phenyl]-3-methyl-1-phenyl-1*H*-pyrazole-5-carboxamide (20)

Yield 66%, white solid. Mp 255–256 °C (EtOAc). 1H NMR (300 MHz, DMSO- d_6) δ 0.76–0.84 (4H, m), 1.84–1.96 (1H, m), 2.29 (3H, s), 6.85 (1H, s), 6.96–7.01 (1H, m), 7.04 (1H, d, $J = 9.6$ Hz), 7.30–7.58 (8H, m), 7.95 (1H, s), 8.03 (1H, d, $J = 9.6$ Hz), 10.64 (1H, s), 11.08 (1H, s). Anal. Calcd for $C_{27}H_{23}N_7O_3 \cdot 0.8H_2O$: C, 63.85; H, 4.88; N, 19.30. Found: C, 63.91; H, 4.97; N, 19.31.

5.1.35. *N*-[3-({2-[(Cyclopropylcarbonyl)amino]imidazo[1,2-*b*]pyridazin-6-yl}oxy)phenyl]-1-methyl-3-(trifluoromethyl)-1*H*-pyrazole-5-carboxamide (21)

Yield 78%, white solid. Mp 249–251 °C (*n*-hexane/EtOAc). 1H NMR (300 MHz, DMSO- d_6) δ 0.73–0.85 (4H, m), 1.84–1.97 (1H, m), 4.15 (3H, s), 7.02–7.10 (2H, m), 7.46 (1H, t, $J = 8.2$ Hz), 7.50 (1H, s), 7.59–7.64 (1H, m), 7.66 (1H, t, $J = 2.1$ Hz), 7.98 (1H, s), 8.06 (1H, d, $J = 9.6$ Hz), 10.53 (1H, s), 11.10 (1H, s). Anal. Calcd for

$C_{22}H_{18}F_3N_7O_3$: C, 54.43; H, 3.74; N, 20.20. Found: C, 54.48; H, 3.75; N, 19.97.

5.1.36. *N*-[6-(3-Amino-4-methylphenoxy)imidazo[1,2-*b*]pyridazin-2-yl]cyclopropanecarboxamide (22a)

A mixture of **8f** (743 mg, 2.3 mmol), 3-amino-4-methylphenol (446 mg, 3.6 mmol), and K_2CO_3 (782 mg, 5.7 mmol) in DMF (6 mL) was stirred at 180 °C for 30 min using a microwave synthesizer. The mixture was concentrated in vacuo. The residue was diluted with water and extracted with EtOAc/THF (1:1). The organic layer was washed with brine, dried over Na_2SO_4 , and filtered. The filtrate was concentrated in vacuo, and the residue was purified by silica gel column chromatography (*n*-hexane/EtOAc 80:20 to 25:75) to give **22a** (424 mg, 58%) as a brown solid. 1H NMR (300 MHz, DMSO- d_6) δ 0.72–0.86 (4H, m), 1.84–1.97 (1H, m), 2.04 (3H, s), 5.06 (2H, s), 6.28 (1H, dd, $J = 8.1, 2.4$ Hz), 6.42 (1H, d, $J = 2.4$ Hz), 6.93 (1H, d, $J = 9.3$ Hz), 6.95 (1H, d, $J = 8.1$ Hz), 7.96 (1H, s), 7.98 (1H, d, $J = 9.3$ Hz), 11.07 (1H, s).

5.1.37. *N*-[6-(5-Amino-2-methylphenoxy)imidazo[1,2-*b*]pyridazin-2-yl]cyclopropanecarboxamide (22b)

To a suspension of NaH (60% in oil, 56 mg, 1.4 mmol) in DMF (2 mL) was added a solution of 5-amino-2-methylphenol (173 mg, 1.4 mmol) in DMF (1 mL), and the mixture was stirred at 0 °C for 30 min. To the mixture was added a solution of **8f** (306 mg, 0.93 mmol) in DMF (1.5 mL), and the mixture was stirred at 110 °C for 24 h. The mixture was concentrated in vacuo. The residue was diluted with water and extracted with EtOAc. The organic layer was washed with brine, dried over Na_2SO_4 , and filtered. The filtrate was concentrated in vacuo, and the residue was purified by silica gel column chromatography (*n*-hexane/EtOAc 83:17 to 10:90) to give **22b** (94 mg, 31%) as a brown solid. 1H NMR (300 MHz, DMSO- d_6) δ 0.73–0.89 (4H, m), 1.84–2.01 (1H, m), 1.97 (3H, s), 5.08 (2H, s), 6.30 (1H, d, $J = 2.3$ Hz), 6.40 (1H, dd, $J = 8.0, 2.3$ Hz), 6.94 (1H, d, $J = 8.0$ Hz), 6.95 (1H, d, $J = 9.5$ Hz), 7.93 (1H, s), 7.99 (1H, d, $J = 9.5$ Hz), 11.06 (1H, s).

5.1.38. *N*-[6-(3-Amino-2-methylphenoxy)imidazo[1,2-*b*]pyridazin-2-yl]cyclopropanecarboxamide (22c)

Compound **22c** was prepared from **8f** and 3-amino-2-methylphenol in a manner similar to that described for **22a**. Yield 58%, brown solid. 1H NMR (300 MHz, DMSO- d_6) δ 0.71–0.87 (4H, m), 1.83–1.98 (1H, m), 1.89 (3H, s), 5.13 (2H, s), 6.32 (1H, d, $J = 8.0$ Hz), 6.55 (1H, d, $J = 6.8$ Hz), 6.93 (1H, dd, $J = 8.0, 6.8$ Hz), 6.94 (1H, d, $J = 9.5$ Hz), 7.91 (1H, s), 7.98 (1H, d, $J = 9.5$ Hz), 11.05 (1H, s).

5.1.39. *N*-[6-(3-Amino-4-ethylphenoxy)imidazo[1,2-*b*]pyridazin-2-yl]cyclopropanecarboxamide (22d)

A mixture of **8f** (984 mg, 3.0 mmol), 3-amino-4-ethylphenol (617 mg, 4.5 mmol), and K_2CO_3 (829 mg, 6.0 mmol) in DMF (9 mL) was stirred at 150 °C for 24 h. The mixture was diluted with water and extracted with EtOAc/THF (3:1). The organic layer was concentrated in vacuo, and the residue was purified by silica gel column chromatography (*n*-hexane/EtOAc 50:50 to 0:100) followed by trituration with EtOAc/*i*-Pr $_2$ O to give **22d** (706 mg, 70%) as a khaki solid. 1H NMR (300 MHz, DMSO- d_6) δ 0.73–0.88 (4H, m), 1.14 (3H, t, $J = 7.4$ Hz), 1.85–2.00 (1H, m), 2.43 (2H, q, $J = 7.4$ Hz), 5.07 (2H, s), 6.31 (1H, dd, $J = 8.1, 2.7$ Hz), 6.42 (1H, d, $J = 2.7$ Hz), 6.93 (1H, d, $J = 9.6$ Hz), 6.95 (1H, d, $J = 7.8$ Hz), 7.97 (1H, s), 7.98 (1H, d, $J = 9.0$ Hz), 11.05 (1H, s).

5.1.40. *N*-[6-(3-Amino-4-fluorophenoxy)imidazo[1,2-*b*]pyridazin-2-yl]cyclopropanecarboxamide (22e)

Compound **22e** was prepared from **8f** and 3-amino-4-fluorophenol in a manner similar to that described for **22d**. Yield 73%,

pale yellow solid. ^1H NMR (300 MHz, DMSO- d_6) δ 0.74–0.86 (4H, m), 1.86–1.98 (1H, m), 5.36 (2H, s), 6.30–6.38 (1H, m), 6.58 (1H, dd, J = 7.7, 2.9 Hz), 6.97 (1H, d, J = 9.6 Hz), 7.03 (1H, dd, J = 11.4, 8.7 Hz), 7.96 (1H, s), 8.00 (1H, dd, J = 9.6, 0.6 Hz), 11.06 (1H, s).

5.1.41. *N*-[6-(3-Amino-4-chlorophenoxy)imidazo[1,2-*b*]pyridazin-2-yl]cyclopropanecarboxamide (22f)

Compound **22f** was prepared from **8f** and 3-amino-4-chlorophenol in a manner similar to that described for **22a**. Yield 73%, brown solid. ^1H NMR (300 MHz, DMSO- d_6) δ 0.72–0.87 (4H, m), 1.84–1.98 (1H, m), 5.56 (2H, s), 6.40 (1H, dd, J = 8.5, 2.8 Hz), 6.61 (1H, d, J = 2.8 Hz), 7.00 (1H, d, J = 9.8 Hz), 7.23 (1H, d, J = 8.5 Hz), 7.98 (1H, s), 8.02 (1H, d, J = 9.8 Hz), 11.09 (1H, s).

5.1.42. *N*-[5-({2-[(Cyclopropylcarbonyl)amino]imidazo[1,2-*b*]pyridazin-6-yl}oxy)-2-methylphenyl]-1,3-dimethyl-1*H*-pyrazole-5-carboxamide (23a)

To an ice-cooled stirred suspension of **22a** (485 mg, 1.50 mmol) in DMA (3 mL) was added 1,3-dimethyl-1*H*-pyrazole-5-carbonyl chloride (262 mg, 1.65 mmol), and the mixture was stirred at room temperature for 15 h. The mixture was diluted with 0.25 N aqueous NaOH and extracted with EtOAc/THF (2:1). The organic layer was washed with water and concentrated in vacuo. The residue was purified by silica gel column chromatography (EtOAc/MeOH 100:0 to 80:20) followed by recrystallization from EtOH to give **23a** (517 mg, 77%) as a white solid. Mp 223 °C. ^1H NMR (300 MHz, DMSO- d_6) δ 0.76–0.85 (4H, m), 1.86–1.98 (1H, m), 2.19 (3H, s), 2.25 (3H, s), 3.97 (3H, s), 6.81 (1H, s), 7.04 (1H, d, J = 9.5 Hz), 7.10 (1H, dd, J = 8.4, 2.5 Hz), 7.27 (1H, d, J = 2.5 Hz), 7.35 (1H, d, J = 8.4 Hz), 7.93 (1H, s), 8.03 (1H, d, J = 9.5 Hz), 9.80 (1H, s), 11.07 (1H, s). Anal. Calcd for $\text{C}_{23}\text{H}_{23}\text{N}_7\text{O}_3$: C, 62.01; H, 5.20; N, 22.01. Found: C, 61.98; H, 5.18; N, 22.08.

5.1.43. *N*-[3-({2-[(Cyclopropylcarbonyl)amino]imidazo[1,2-*b*]pyridazin-6-yl}oxy)-4-methylphenyl]-1,3-dimethyl-1*H*-pyrazole-5-carboxamide (23b)

To an ice-cooled stirred solution of **22b** (73 mg, 0.23 mmol) in THF (5 mL) were added Et_3N (68 mg, 0.67 mmol) and 1,3-dimethyl-1*H*-pyrazole-5-carbonyl chloride (46 mg, 0.29 mmol), and the mixture was stirred at room temperature for 1 h. The mixture was diluted with saturated aqueous NaHCO_3 and extracted with EtOAc. The organic layer was washed with brine, dried over Na_2SO_4 , and filtered. The filtrate was concentrated in vacuo to a volume of approximately 1 mL, and the precipitate was collected by filtration and washed with *n*-hexane/EtOAc to give **23b** (64 mg, 64%) as a white solid. Mp 137 °C. ^1H NMR (300 MHz, DMSO- d_6) δ 0.70–0.88 (4H, m), 1.85–1.97 (1H, m), 2.14 (3H, s), 2.18 (3H, s), 3.97 (3H, s), 6.81 (1H, s), 7.08 (1H, d, J = 9.5 Hz), 7.32 (1H, d, J = 8.3 Hz), 7.55 (1H, dd, J = 8.3, 1.9 Hz), 7.60 (1H, d, J = 1.9 Hz), 7.92 (1H, s), 8.05 (1H, d, J = 9.5 Hz), 10.18 (1H, s), 11.08 (1H, s). Anal. Calcd for $\text{C}_{23}\text{H}_{23}\text{N}_7\text{O}_3 \cdot 1.5\text{H}_2\text{O}$: C, 58.47; H, 5.55; N, 20.75. Found: C, 58.40; H, 5.56; N, 20.69.

5.1.44. *N*-[3-({2-[(Cyclopropylcarbonyl)amino]imidazo[1,2-*b*]pyridazin-6-yl}oxy)-2-methylphenyl]-1,3-dimethyl-1*H*-pyrazole-5-carboxamide (23c)

Compound **23c** was prepared from **22c** in a manner similar to that described for **23b**. Yield 82%, white solid. Mp 262 °C (*n*-hexane/EtOAc). ^1H NMR (300 MHz, DMSO- d_6) δ 0.72–0.87 (4H, m), 1.86–1.98 (1H, m), 2.06 (3H, s), 2.20 (3H, s), 4.01 (3H, s), 6.84 (1H, s), 7.09 (1H, d, J = 9.5 Hz), 7.15 (1H, dd, J = 6.8, 2.3 Hz), 7.25–7.36 (2H, m), 7.88 (1H, s), 8.05 (1H, d, J = 9.5 Hz), 9.95 (1H, s), 11.07 (1H, s). Anal. Calcd for $\text{C}_{23}\text{H}_{23}\text{N}_7\text{O}_3 \cdot 0.3\text{H}_2\text{O}$: C, 61.27; H, 5.28; N, 21.75. Found: C, 61.31; H, 5.03; N, 21.51.

5.1.45. *N*-[5-({2-[(Cyclopropylcarbonyl)amino]imidazo[1,2-*b*]pyridazin-6-yl}oxy)-2-ethylphenyl]-1,3-dimethyl-1*H*-pyrazole-5-carboxamide (23d)

To a stirred solution of **22d** (202 mg, 0.60 mmol) in NMP (3 mL) was added 1,3-dimethyl-1*H*-pyrazole-5-carbonyl chloride (143 mg, 0.90 mmol), and the mixture was stirred at room temperature for 8 h. The mixture was diluted with 1 N aqueous NaOH and extracted with EtOAc. The organic layer was concentrated in vacuo, and the residue was purified by silica gel column chromatography (EtOAc/MeOH 100:0 to 80:20) followed by recrystallization from EtOAc/*i*-Pr₂O to give **23d** (167 mg, 61%) as a white solid. Mp 199 °C. ^1H NMR (300 MHz, DMSO- d_6) δ 0.76–0.84 (4H, m), 1.15 (3H, t, J = 7.6 Hz), 1.84–2.00 (1H, m), 2.19 (3H, s), 2.63 (2H, q, J = 7.6 Hz), 3.97 (3H, s), 6.80 (1H, s), 7.04 (1H, d, J = 9.6 Hz), 7.15 (1H, dd, J = 8.6, 2.6 Hz), 7.23 (1H, d, J = 2.6 Hz), 7.37 (1H, d, J = 8.6 Hz), 7.94 (1H, s), 8.03 (1H, dd, J = 9.6, 0.6 Hz), 9.82 (1H, s), 11.07 (1H, s). Anal. Calcd for $\text{C}_{24}\text{H}_{25}\text{N}_7\text{O}_3 \cdot 0.3\text{H}_2\text{O}$: C, 62.00; H, 5.55; N, 21.09. Found: C, 61.95; H, 5.51; N, 21.09.

5.1.46. *N*-[5-({2-[(Cyclopropylcarbonyl)amino]imidazo[1,2-*b*]pyridazin-6-yl}oxy)-2-fluorophenyl]-1,3-dimethyl-1*H*-pyrazole-5-carboxamide (23e)

To an ice-cooled stirred solution of **22e** (1.64 g, 5.0 mmol) in DMA (30 mL) was added a solution of 1,3-dimethyl-1*H*-pyrazole-5-carbonyl chloride (0.83 g, 5.2 mmol) in DMA (5 mL), and the mixture was stirred at room temperature for 1.5 h. The mixture was diluted with aqueous NaHCO_3 under ice cooling and extracted with EtOAc. The organic layer was washed with brine, dried over MgSO_4 , and filtered. The filtrate was concentrated in vacuo, and the residue was purified by silica gel column chromatography (EtOAc/MeOH 100:0 to 95:5) followed by recrystallization from EtOAc/MeOH to give a pale yellow solid (1.82 g). The solid was recrystallized from EtOH/THF to give **23e** (1.48 g, 66%) as a white solid. Mp 234 °C. ^1H NMR (300 MHz, DMSO- d_6) δ 0.72–0.88 (4H, m), 1.84–2.00 (1H, m), 2.19 (3H, s), 3.97 (3H, s), 6.84 (1H, s), 7.07 (1H, d, J = 9.6 Hz), 7.14–7.25 (1H, m), 7.39 (1H, t, J = 9.6 Hz), 7.48–7.58 (1H, m), 7.93 (1H, s), 8.03 (1H, d, J = 9.6 Hz), 10.09 (1H, s), 11.06 (1H, s). Anal. Calcd for $\text{C}_{22}\text{H}_{20}\text{FN}_7\text{O}_3$: C, 58.79; H, 4.49; N, 21.82. Found: C, 58.61; H, 4.44; N, 21.74.

5.1.47. *N*-[2-Chloro-5-({2-[(cyclopropylcarbonyl)amino]imidazo[1,2-*b*]pyridazin-6-yl}oxy)phenyl]-1,3-dimethyl-1*H*-pyrazole-5-carboxamide (23f)

Compound **23f** was prepared from **22f** in a manner similar to that described for **23e** to yield 66% as a white solid. Mp 255 °C (EtOH/THF). ^1H NMR (300 MHz, DMSO- d_6) δ 0.72–0.86 (4H, m), 1.85–1.98 (1H, m), 2.20 (3H, s), 3.98 (3H, s), 6.84 (1H, s), 7.10 (1H, d, J = 9.6 Hz), 7.26 (1H, dd, J = 8.9, 2.8 Hz), 7.54 (1H, d, J = 2.8 Hz), 7.64 (1H, d, J = 8.9 Hz), 7.96 (1H, s), 8.06 (1H, d, J = 9.6 Hz), 9.99 (1H, s), 11.09 (1H, s). Anal. Calcd for $\text{C}_{22}\text{H}_{20}\text{ClN}_7\text{O}_3$: C, 56.72; H, 4.33; Cl, 7.61; N, 21.04. Found: C, 56.65; H, 4.30; Cl, 7.51; N, 21.03.

5.2. X-ray crystal structure determination

Purified VEGFR2 kinase domain was prepared as described previously.³¹ Prior to crystallization with **19**, 10 mg/mL of the enzyme was incubated with 1 mM of **19** on ice for 1 hour, followed by centrifugation to remove precipitation. The given enzyme/inhibitor complex was crystallized by sitting drop vapor diffusion method under the condition of a 1:1 mixture of the protein solution with the reservoir solution of 0.1 M HEPES pH 8.5, 1.2 M tri-sodium citrate. Crystals were harvested by mixing with the cryoprotectant ethylene glycerol to a final concentration of 25% in mother liquor and flash-frozen by direct immersion in liquid nitrogen. X-ray dif-

fraction data were collected at the Advanced Light Source (ALS) beamline 5.0.3 (Berkeley, CA), and processed using the program HKL2000.³² The crystal was diffracted to 1.52 Å, providing an unambiguous electron density for **19**. The structure was determined by molecular replacement using MOLREP,³³ utilizing the previously reported coordinate of VEGFR2 with the PDB accession code 3VHE.³¹ Subsequently, structure refinement and model building were performed utilizing REFMAC.³⁴ The solved structure was modeled with WinCoot (version 0.3.3).³⁵

5.3. VEGFR2 kinase inhibition assay

The kinase activity of VEGFR2 was measured by use of an anti-phosphotyrosine antibody with the AlphaScreen® system (Perkin-Elmer, USA). Enzyme reactions were performed in 50 mM Tris-HCl pH 7.5, 5 mM MnCl₂, 5 mM MgCl₂, 0.01% Tween-20 and 2 mM DTT, containing 10 μM ATP, 0.1 μg/mL biotinylated poly-GluTyr (4:1) and 0.1 nM of VEGFR2 (Millipore, UK). Prior to catalytic initiation with ATP, compound and enzyme were incubated for 5 min at room temperature (preincubation). The reactions were quenched by the addition of 25 μL of 100 mM EDTA, 10 μg/mL AlphaScreen streptavidine donor beads and 10 μg/mL acceptor beads in 62.5 mM HEPES pH 7.4, 250 mM NaCl, and 0.1% BSA. Plates were incubated in the dark overnight and then read by EnVision 2102 Multilabel Reader (PerkinElmer, USA). Wells containing the substrate and the enzyme without compound were used as total reaction control. Wells containing biotinylated poly-GluTyr (4:1) and enzyme without ATP were used as basal control. The concentration of inhibitor producing 50% inhibition of the kinase activities (IC₅₀ values) and 95% confidence intervals (95% CI) were analyzed using GraphPad Prism version 5.01, GraphPad Software (USA). Sigmoidal dose–response (variable slope) curves were fitted using non-linear regression analysis, with the top and bottom of the curve constrained at 100 and 0, respectively.

For time-dependent inhibition analyses, enzyme assays were performed with the same method as above in four conditions; 10 μM ATP with 5 min of preincubation, 10 μM ATP with 60 min of preincubation, 1 mM ATP with 5 min of preincubation and 1 mM ATP with 60 min of preincubation. Each assay was performed in at least duplicate.

5.4. Cell growth inhibition assay

HUVECs (Cambrex, USA) were seeded into a 96-well plate at 3000 cells/well in Human Endothelial-SFM Growth Medium (Invitrogen) containing 3% fetal bovine serum (FBS) (Hyclone, USA) and were incubated overnight at 37 °C in a 5% CO₂ incubator. Various concentrations of the test compounds were added in the presence of 60 ng/mL VEGF (R&D systems, USA), and the cells were cultured for a further 5 days. Cellular proliferation was determined by the WST-8 formazan assay using Cell Counting Kit-8 (DOJINDO Laboratories, Japan). Briefly, 10 μL/well of Cell Counting Kit-8 was added and the cells were cultured for several hours. Then, the absorbance value at 450 nm was measured using a Benchmark Plus Microplate reader (Bio-Rad Labs., USA). The IC₅₀ values and 95% confidence intervals (95% CI) were calculated from a dose–response curve generated by least-squares linear regression of the response using NLIN procedure of the SAS software (SAS Institute Japan, Inc., Japan).

5.5. Pharmacokinetic studies in mice using cassette dosing

Test compounds were administered at a dose of 10 mg/kg as a cassette dosing to nonfasted mice (BALB/cAJcl; female; CLEA Japan, Inc.). After oral administration, blood samples were collected. The blood samples were centrifuged to obtain the plasma fraction. The plasma samples were deproteinized with acetonitrile contain-

ing an internal standard. After centrifugation, the supernatant was diluted with a mixture of 0.01 mol/L ammonium formate solution and acetonitrile (9:1, v/v) and centrifuged again. The compound concentrations in the supernatant were measured by LC/MS/MS.

5.6. Metabolic stability assay

Human and mouse liver microsomes were purchased from Xenotech, LLC (Lenexa, KS). An incubation mixture consisted of microsomes in 50 mmol/L KH₂PO₄/K₂HPO₄ buffer (pH 7.4) and 1 μmol/L test compound. The concentration of microsomes was 0.2 mg protein/mL. An NADPH-generating system containing 25 mmol/L MgCl₂, 25 mmol/L glucose-6-phosphate, 2.5 mmol/L beta-NADP⁺ and 7.5 unit/mL glucose-6-phosphate dehydrogenase was added to the incubation mixture with a 20% volume of the reaction mixture to initiate the enzyme reaction. After the addition of the NADPH-generating system, the mixture was incubated at 37 °C. The reaction was terminated by the addition of acetonitrile equivalent to the volume of the reaction mixture. Test compound in the reaction mixture was measured by HPLC equipped with a UV detector or LC/MS/MS. For metabolic stability determinations, chromatograms were analyzed for parent compound disappearance from the reaction mixtures.

5.7. Solubility measurement

Solubility was measured by concentration quantification of the filtrate of a suspension including drug substance and aqueous solution after shaking for 18 h at 37 °C. The quantification was performed by HPLC equipped with a photo diode array detector.

5.8. Pharmacokinetic studies in rats and monkeys

The animals used in this study were male albino rats (CrI:CD(SD) rat; weight, 278.2–313.4 g; Charles River Laboratories Japan, Inc., Ibaraki, Japan) and male cynomolgus monkeys (weight, 2.53–3.27 kg; Keiari Co., Ltd., Wakayama, Japan).

Compound **23a** was suspended in 0.5% (weight/vol) methylcellulose solution for oral (po) administration at the doses of 0.5 mg/10 mL/kg to rats or 0.5 mg/2 mL/kg to monkeys. **23a** was dissolved in mixture of dimethylacetamide/saline (1:1, by vol) for intravenous (iv) injection at the doses of 0.25 mg/mL/kg to rats or 0.25 mg/0.2 mL/kg to monkeys. The formulated test compound was administered to nonfasted rats or fed monkeys. The iv administration in rats was conducted under anesthesia with diethyl ether. At 5, 10 (only for iv dosing), 15, 30 min, and 1, 2, 3, 4, 6, 8, 12, 24, 32 (only for monkeys) and 48 h (only for monkeys) after dosing, blood was taken from the tail vein in rats or from the femoral vein in monkeys. Then, the blood was centrifuged to obtain the plasma fraction. The plasma was kept frozen at –20 °C until analysis.

The concentration of **23a** in plasma was determined by the high-performance liquid chromatography with a fluorescence detector. The excitation and emission were 346 and 420 nm, respectively.

Data were expressed as the mean values with standard deviations (SD) for the results of three to four animals, unless otherwise indicated. Values for maximum plasma concentration (C_{max}) and time to reach C_{max} (T_{max}) were noted directly from the data. The area under the plasma concentration–time curve from 0 to 24 or 48 h after administration (AUC_{0–24h} or AUC_{0–48h}), plasma clearance (CL_{tot}), volume of distribution at steady state (V_{dss}) and mean residence time (MRT) were calculated by the non-compartmental model using WinNonlin Ver.4.1 (Pharsight Corporation). The AUC was calculated by the trapezoidal rule. The bioavailability (BA) was determined after dose normalization.

5.9. Xenograft model antitumor assay

Human lung carcinoma cell line A549 (ATCC No. CCL-185) was obtained from American Type Culture Collection (Manassas, USA). The cells were proliferated in DMEM (Invitrogen, Carlsbad, USA) supplemented with 10% heat-inactivated fetal bovine serum (HyClone, Logan, USA) and antibiotics (100 units/mL penicillin G and 100 µg/mL streptomycin, Wako Pure Chemical, Japan). The cells were cultured in tissue culture dishes in a humidified incubator at 37 °C in an atmosphere of 5% CO₂ and 95% air. Compound was suspended in 0.5 w/v% methylcellulose (Shin-Etsu Chemical, Japan) vehicle solution. Six-week old female athymic nude mice (BALB/cA/Jcl-nu/nu, CLEA Japan, Japan) received subcutaneous injections into the hind flank with 5×10^6 A549 cells in 100 µL of Hanks' balanced salt solution (Invitrogen). When tumors reached a volume of 100–150 mm³, mice were randomized into four groups ($n = 5$). Then, mice were orally given vehicle or compound (0.25, 1, and 4 mg/kg) twice-daily for 2 weeks. Tumor volumes were assessed by bilateral vernier caliper measurement twice-weekly after inoculation and calculated as volume = length \times width² \times 1/2, where length was taken to be the longest diameter across the tumor and width the corresponding perpendicular. Treatment over control (T/C, %), an index of antitumor efficacy, was calculated by comparison of the mean change in tumor volume over the treatment period for the control and treated groups. Body weight was also measured on the day of tumor volume assessment. Effects of compound on tumor growth and body weight were statistically analyzed by a one-tailed Williams' test or Shirley–Williams' test. Differences were considered significant at $p \leq 0.025$.

Acknowledgments

The authors would like to thank Ms. T. Yoshida for kinase assay; Dr. A. Mizutani, Mr. Y. Nagase, and Dr. K. Nakamura for pharmacological in vitro and in vivo assays; Dr. K. Iwamoto and Ms. A. Hirokawa for protein production for X-ray crystallography; Ms. Y. Watanabe for PK evaluation; Dr. K. Kamiyama and Dr. T. Kitazaki for helpful discussion and supports; and all TAK-593 project team members for their valuable contributions.

Supplementary data

Supplementary data associated with this article can be found, in the online version, at <http://dx.doi.org/10.1016/j.bmc.2013.01.074>. These data include MOL files and InChIKeys of the most important compounds described in this article.

References and notes

- (a) Folkman, J. *N. Engl. J. Med.* **1971**, 285, 1182; (b) Folkman, J.; Shing, Y. *J. Biol. Chem.* **1992**, 267, 10931.
- Shibuya, M.; Claesson-Welsh, L. *Exp. Cell Res.* **2006**, 312, 549.
- (a) Dougher, M.; Terman, B. I. *Oncogene* **1999**, 18, 1619; (b) Hubbard, S. R. *Prog. Biophys. Mol. Biol.* **1999**, 71, 343; (c) Strawn, L. M.; Shawver, L. K. *Expert Opin. Investig. Drugs* **1998**, 7, 553.
- Yoshiji, H.; Kuriyama, S.; Hicklin, D. J.; Huber, J.; Yoshii, J.; Miyamoto, Y.; Kawata, M.; Ikenaka, Y.; Nakatani, T.; Tsujinoue, H.; Fukui, H. *Hepatology* **1999**, 30, 1179.
- Crew, J. P.; O'Brien, T.; Bradburn, M.; Fuggle, S.; Bicknell, R.; Cranston, D.; Harris, A. L. *Cancer Res.* **1997**, 57, 5281.
- Balbay, M. D.; Pettaway, C. A.; Kuniyasu, H.; Inoue, K.; Ramirez, E.; Li, E.; Fidler, I. J.; Dinney, C. P. N. *Clin. Cancer Res.* **1999**, 5, 783.
- Samoto, K.; Ikezaki, K.; Ono, M.; Shono, T.; Kohno, K.; Kuwano, M.; Fukui, M. *Cancer Res.* **1995**, 55, 1189.
- Takahashi, A.; Sasaki, H.; Kim, S. J.; Tobisu, K.; Kakizoe, T.; Tsukamoto, T.; Kumamoto, Y.; Sugimura, T.; Terada, M. *Cancer Res.* **1994**, 54, 4233.
- Guetz, G. D.; Uzzan, B.; Nicolas, P.; Cucherat, M.; Morere, J. F.; Benamouzig, R.; Breaux, J. L.; Perret, G. Y. *Br. J. Cancer* **2006**, 94, 1823.
- Yuan, A.; Yu, C. J.; Chen, W. J.; Lin, F. Y.; Kuo, S. H.; Luh, K. T.; Yang, P. C. *Int. J. Cancer* **2000**, 89, 475.
- Jacobsen, J.; Grankvist, K.; Rasmussen, T.; Bergh, A.; Landberg, G.; Ljungberg, B. *Br. J. Urol. Int.* **2004**, 93, 297.
- Ferrara, N.; Hillan, K. J.; Gerber, H. P.; Novotny, W. *Nat. Rev. Drug Disc.* **2004**, 3, 391.
- Strumberg, D. *Drugs Today* **2005**, 41, 773.
- Motzer, R. J.; Michaelson, M. D.; Redman, B. G.; Hudes, G. R.; Wilding, G.; Figlin, R. A.; Ginsberg, M. S.; Kim, S. T.; Baum, C. M.; DePrimo, S. E.; Li, J. Z.; Bello, C. L.; Theuer, C. P.; George, D. J.; Rini, B. I. *J. Clin. Oncol.* **2006**, 24, 16.
- Harris, P. A.; Bolor, A.; Cheung, M.; Kumar, R.; Crosby, R. M.; Davis-Ward, R. G.; Epperly, A. H.; Hinkle, K. W.; Hunter, R. N., III; Johnson, J. H.; Knick, V. B.; Laudeman, C. P.; Luttrell, D. K.; Mook, R. A.; Nolte, R. T.; Rudolph, S. K.; Szwedczyk, J. R.; Truesdale, A. T.; Veal, J. M.; Wang, L.; Stafford, J. A. *J. Med. Chem.* **2008**, 51, 4632.
- Rini, B. I.; Escudier, B.; Tomczak, P.; Kaprin, A.; Szczylik, C.; Hutson, T. E.; Michaelson, M. D.; Gorbunova, V. A.; Gore, M. E.; Rusakov, I. G.; Negrier, S.; Ou, Y. C.; Castellano, D.; Lim, H. Y.; Uemura, H.; Tarazi, J.; Cella, D.; Chen, C.; Rosbrook, B.; Kim, S.; Motzer, R. J. *Lancet* **2011**, 378, 1931.
- (a) Roth, G. J.; Heckel, A.; Colbatzky, F.; Handschuh, S.; Kley, J.; Lehmann-Lintz, T.; Lotz, R.; Tontsch-Grunt, U.; Walter, R.; Hilberg, F. *J. Med. Chem.* **2009**, 52, 4466; (b) Renhowe, P. A.; Pecchi, S.; Shafer, C. M.; Machajewski, T. D.; Jazan, E. M.; Taylor, C.; Antonios-McCrea, W.; McBride, C. M.; Frazier, K.; Wiesmann, M.; Lapointe, G. R.; Feucht, P. H.; Warne, R. L.; Heise, C. C.; Menezes, D.; Aardalen, K.; Ye, H.; He, M.; Le, V.; Vora, J.; Jansen, J. M.; Wernette-Hammond, M. E.; Harris, A. L. *J. Med. Chem.* **2009**, 52, 278; (c) Polverino, A.; Coxon, A.; Starnes, C.; Diaz, Z.; DeMelfi, T.; Wang, L.; Bradley, J.; Estrada, J.; Cattley, R.; Kaufman, S.; Chen, D.; Gan, Y.; Kumar, G.; Meyer, J.; Neervannan, S.; Alva, G.; Talvenheim, J.; Montestruque, S.; Tasker, A.; Patel, V.; Radinsky, R.; Kendall, R. *Cancer Res.* **2006**, 66, 8715; (d) Nakamura, K.; Taguchi, E.; Miura, T.; Yamamoto, A.; Takahashi, K.; Bichat, F.; Guilbaud, N.; Hasegawa, K.; Kubo, K.; Fujiwara, Y.; Suzuki, R.; Kubo, K.; Shibuya, M.; Isae, T. *Cancer Res.* **2006**, 66, 9134; (e) Dai, Y.; Hartandi, K.; Ji, Z.; Ahmed, A. A.; Albert, D. H.; Bauch, J. L.; Bouska, J. J.; Bousquet, P. F.; Cunha, G. A.; Glaser, K. B.; Harris, C. M.; Hickman, D.; Guo, J.; Li, J.; Marcotte, P. A.; Marsh, K. C.; Moskey, M. D.; Martin, R. L.; Olson, A. M.; Osterling, D. J.; Pease, L. J.; Soni, N. B.; Stewart, K. D.; Stoll, V. S.; Tapang, P.; Reuter, D. R.; Davidsen, S. K.; Michaelides, M. R. *J. Med. Chem.* **2007**, 50, 1584; (f) Bold, G.; Altmann, K. H.; Frei, J.; Lang, M.; Manley, P. W.; Traxler, P.; Wietfeld, B.; Brügggen, J.; Buchdunger, E.; Cozens, R.; Ferrari, S.; Furet, P.; Hofmann, F.; Martiny-Baron, G.; Mestan, J.; Rösel, J.; Sills, M.; Stover, D.; Acemoglu, F.; Boss, E.; Emmenegger, R.; Lässer, L.; Masso, E.; Roth, R.; Schlachter, C.; Vetterli, W.; Wyss, D.; Wood, J. M. *J. Med. Chem.* **2000**, 43, 2310; (g) Gingrich, D. E.; Reddy, D. R.; Iqbal, M. A.; Singh, J.; Aimone, L. D.; Angeles, T. S.; Albom, M.; Yang, S.; Ator, M. A.; Meyer, S. L.; Robinson, C.; Ruggeri, B. A.; Dionne, C. A.; Vaught, J. L.; Mallamo, J. P.; Hudkins, R. L. *J. Med. Chem.* **2003**, 46, 5375; (h) Cai, Z. W.; Zhang, Y.; Borzilleri, R. M.; Qian, L.; Barbosa, S.; Wei, D.; Zheng, X.; Wu, L.; Fan, J.; Shi, Z.; Wautlet, B. S.; Mortillo, S.; Jeyaseelan, R.; Sr.; Kukral, D. W.; Kamath, A.; Marathe, P.; D'Arienzo, C.; Derbin, G.; Barrish, J. C.; Robl, J. A.; Hunt, J. T.; Lombardo, L. J.; Fargnoli, J.; Bhude, R. S. *J. Med. Chem.* **2008**, 51, 1976.
- (a) Abramsson, A.; Lindblom, P.; Betsholtz, C. *J. Clin. Invest.* **2003**, 112, 1142; (b) Lindahl, P.; Johansson, B. R.; Lévee, P.; Betsholtz, C. *Science* **1997**, 277, 242.
- Bergers, G.; Song, S.; Meyer-Morse, N.; Bergsland, E.; Hanahan, D. *J. Clin. Invest.* **2003**, 111, 1287.
- Pietras, K.; Sjöblom, T.; Rubin, K.; Heldin, C. H.; Ostman, A. *Cancer Cell* **2003**, 3, 439.
- Miyamoto, N.; Oguro, Y.; Takagi, T.; Iwata, H.; Miki, H.; Hori, A.; Imamura, S. *Bioorg. Med. Chem.* **2012**, 20, 7051.
- The fragment library screening was performed by an enzyme inhibition assay using VEGFR2 kinase domain, which was used in X-ray crystallography. Compound **3** was identified as one of the hit fragments with an IC₅₀ value of 34 µM.
- Ullman, E. F.; Kirakossian, H.; Singh, S.; Wu, Z. P.; Irvin, B. R.; Pease, J. S.; Switchenko, A. C.; Irvine, J. D.; Dafforn, A.; Skold, C. N.; Wagner, D. B. *Proc. Natl. Acad. Sci. U.S.A.* **1994**, 91, 5426.
- Liu, Y.; Gray, N. S. *Nat. Chem. Biol.* **2006**, 2, 358.
- Iwata, H.; Imamura, S.; Hori, A.; Hixon, M. S.; Kimura, H.; Miki, H. *Biochemistry* **2011**, 50, 738.
- Lipinski, C. A.; Lombardo, F.; Dominy, B. W.; Feeney, P. J. *Adv. Drug Delivery Rev.* **2001**, 46, 3.
- Ishikawa, M.; Hashimoto, Y. *J. Med. Chem.* **2011**, 54, 1539.
- Awazu, Y.; Mizutani, A.; Nagase, Y.; Tsuchiya, S.; Nakamura, K.; Kakoi, Y.; Kitahara, O.; Takeuchi, T.; Yamasaki, S.; Miyamoto, N.; Iwata, H.; Miki, H.; Imamura, S.; Hori, A. *Cancer Sci.* **2013**, <http://dx.doi.org/10.1111/cas.12101>.
- Tummino, P. J.; Copeland, R. A. *Biochemistry* **2008**, 47, 5481.
- Maes, B. U. W.; Lemièr, G. L. F.; Dommissie, R.; Augustyns, K.; Haemers, A. *Tetrahedron* **2000**, 56, 1777.
- Oguro, Y.; Miyamoto, N.; Okada, K.; Takagi, T.; Iwata, H.; Awazu, Y.; Miki, H.; Hori, A.; Kamiyama, K.; Imamura, S. *Bioorg. Med. Chem.* **2010**, 18, 7260.
- Otwinowski, Z.; Minor, W. *Methods Enzymol.* **1997**, 276, 307.
- Vagin, A.; Teplyakov, A. *J. Appl. Crystallogr.* **1997**, 30, 1022.
- Collaborative Computational Project, Number 4. The CCP4 suite: programs for protein crystallography. *Acta Crystallogr., Sect. D: Biol. Crystallogr.* **1994**, 50, 760.
- Emsley, P.; Lohkamp, B.; Scott, W. G.; Cowtan, K. *Acta Crystallogr., Sect. D: Biol. Crystallogr.* **2010**, 66, 486.